Chemically programmed metabolism drives a superior cell fitness for cartilage regeneration

Chemically programmed metabolism drives a superior cell fitness for cartilage regeneration

Yishan Chen[1,2,3†], Yiyang Yan[1,2,3†], Ruonan Tian[3], Zixuan Sheng[2], Liming Li[5], Jiachen Chen[6], Yuan Liao[7], Ya Wen[1,2], Junting Lu[3], Xinyu Liu[3], Wei Sun[1,2,3], Haoyu Wu[1,2], Youguo Liao[1,2], Xianzhu Zhang[8], Xuri Chen[1,2], Chengrui An[2], Kun Zhao[2], Wanlu Liu[3], Jianqing Gao[6], David C. Hay[9], and Hongwei Ouyang[1,2,3,4*]

1. Department of Sports Medicine of the Second Affiliated Hospital, and Liangzhu Laboratory, Zhejiang University School of Medicine, Hangzhou, China.

2. Dr. Li Dak Sum & Yip Yio Chin Center for Stem Cells and Regenerative Medicine, Zhejiang University School of Medicine, Hangzhou, China.

3. Zhejiang University-University of Edinburgh Institute, Zhejiang University School of Medicine, Haining, China.

4. China Orthopedic Regenerative Medicine Group (CORMed), Hangzhou, China.

5. Rehabilitation Sciences and Engineering, University of Health and Rehabilitation Sciences, Qingdao, China.

6. College of Pharmaceutical Sciences, Zhejiang University, Hangzhou, China.

7. Center for Stem Cell and Regenerative Medicine, and Bone Marrow Transplantation Center, The First Affiliated Hospital, Zhejiang University School of Medicine, Hangzhou, China.

8. Department of Orthopedics, The First Affiliated Hospital, Zhejiang University School of Medicine, Hangzhou, China.

9. Centre for Regenerative Medicine, Institute for Regeneration and Repair, The University of Edinburgh, Edinburgh, United Kingdom.

*Correspondence author. Email: hwoy@zju.edu.cn; Fax/Phone: +86-571-88208262

†These authors contributed equally to this work.

Teaser: We propose a cost-effective chemical strategy to induce energetic super-fit chondrocytes for human cartilage regeneration.

Abstract

The rapid advancement of cell therapies underscores the importance of understanding fundamental cellular attributes. Among these, cell fitness—how transplanted cells adapt to new microenvironments and maintain functional stability in vivo—is crucial. This study identifies a chemical compound, FPH2, that enhances the fitness of human chondrocytes and the repair of articular cartilage, which is typically non-regenerative. Through drug screening, FPH2 was shown to broadly improve cell performance, especially in maintaining chondrocyte phenotype and enhancing migration. Single-cell transcriptomics indicated that FPH2 induced a super-fit cell state. The mechanism primarily involves the inhibition of carnitine palmitoyl transferase I and the optimization of metabolic homeostasis. In animal models, FPH2-treated human chondrocytes significantly improved cartilage regeneration, demonstrating well-integrated tissue interfaces in rats. Additionally, an acellular FPH2-loaded hydrogel proved effective in preventing the onset of osteoarthritis. This research provides a viable and safe method to enhance chondrocyte fitness, offering insights into the self-regulatory mechanisms of cell fitness.

Introduction

Cell therapy has been proposed as a scalable modality to treat human diseases, using functional cellular transplants to modulate tissue pathology and restore normal bodily functions *(1)*. This requires a good scientific understanding of the fundamental features that determine cell performance in vivo *(2)*. Among them, cell fitness, representing the ability to engraft, adapt, proliferate and function in a new environment, is the key to graft performance. A good example of this is the use of engineered T cells for treating hematologic malignancies. Their therapeutical efficacy has been shown to largely rely on the fitness of transferred T cells, in other words, their survival and the ability to renovate antitumor immunity in vivo *(2)*. Besides these lessons, increasing evidences have illustrated that a controllably high level of cell fitness could maximize the efficacy of cell therapy in tissue regeneration *(2-4)*. In these conditions, only winner cells are predicted to thrive and initiate the self-renewal procedure, while less-fit cells will be eliminated *(5, 6)*. Therefore, cell fitness is regarded as the core of maintaining cell function and homeostasis in changeable environments, and manipulating pre-implantation cell fitness may become a reliable strategy to guarantee the cells' ability to complete the desirable tasks for tissue regeneration and repair.

Unfortunately, compromised cell fitness is observed in failed regeneration of human tissues. For example, human adult chondrocytes in articular cartilage, are typically less-fit cells with poor self-regenerative potential. They mostly display dysfunctional cell proliferation or matrix secretion in improperly treated injuries, which may ultimately lead to cartilage degeneration *(7, 8)*. Over time this culminates in the development and progression of osteoarthritis (OA), currently affecting over 500 million people globally *(9)*. Additionally, poor cell fitness of chondrocytes is also observed post ex-vivo isolation. In particular, freshly isolated primary chondrocytes were not able to adapt to the in vitro culture environment, and lost their phenotype rapidly. This process is defined as chondrocyte dedifferentiation, which usually became irreversible following cell expansion beyond passage four (P4), and was even accompanied by an arrest of proliferation at later stages *(10)*. This phenomenon has been shown to compromise the outcomes of chondrocyte pre-implantation culture for the treatment of cartilage injuries *(11)*. However, due to the lack of understanding on the regulatory genes that underpin human chondrocyte fitness, it is still difficult to effectively modulate those cells for tissue regeneration. Although some molecular targets, such as Myc, were highlighted in other studies *(4)*, such strategies have not been widely applied in the field. The

genetic signals regulating cell fitness also vary by species, tissue types and cell subpopulations *(3, 12)*. Moreover, safety concerns may also arise, because the reported target genes were shown to be deeply involved in oncogenic pathways *(13, 14)*. Therefore, there is still an urgent need to develop safe and cost-effective therapeutics to manipulate cell fitness for human tissue regeneration and repair.

With this in mind, small molecular chemical compounds have been successfully deployed to finely tune protein function without induing oncogenic genes *(15)*. Additionally, other studies have reported that they are powerful tools to drive cell fate decisions and maintain biological phenotypes *(16, 17)*, and are widely adopted with distinct advantages in manufacture, storage, transportation and standardization. Our previous study has dissected the dynamic changes in chondrocyte biology and their adaptative behaviors during ex-vivo monolayer culture *(10)*. In this study, we used this biological model as a screen platform, which provided quantitative parameters including cell proliferative rate and functional phenotype levels during cell culture, to discover new drugs that regulated chondrocyte fitness, with the rationale that hits from this screen could be useful for both in vitro and in vivo endeavors. We identified that the compound FPH2 significantly improved chondrocyte functional performance in different adverse conditions. Single-cell analysis confirmed that FPH2 induced a winner energetic cell status, with high levels of adaptive responsive gene expression. We then revealed that FPH2's mechanism of action centered on the inhibition of carnitine palmitoyl transferase I, which resulted in a modified metabolic pattern, and optimized mitochondrial homeostasis. In vivo, FPH2 pretreated-human chondrocytes exhibited a stronger ability to maintain tissue function and integrate with surrounding tissues. Moreover, FPH2-loaded acellular hydrogels could protect the joint surfaces from OA in rats. Overall, we provide a safe, convenient and cost-effective chemical strategy to induce the regenerative capacity of human chondrocytes, and their in vivo niche, in order to drive better tissue repair.

Results

High-throughput screening to discover compounds driving chondrocyte cell fitness

We hypothesized that chemical compounds could manipulate cell fitness, and to study this in detail we deployed our chondrocyte fitness model *(10)*. In this model, we adopted the phenomenon that chondrocytes would become dysfunctional after leaving their in vivo niche, showing a decline of proliferation rate and a loss of lineage phenotype during cell passaging in normoxic conditions

(21% O_2) (Fig. 1A). We defined cells with a higher fitness (winner cells) as those that exhibited slower rates of proliferative/phenotypic decline in monolayer culture, and a faster recovery in redifferentiation induction experiments (Fig. 1B). In these experiments, we used Col2-pd2EGFP reporter chondrocytes *(18)* in combination with a high-throughput/content imaging system (YOKOGAWA CQ1), to quantify both proliferative rate and functional phenotype maintenance (Fig. 1C). After a 48-hour treatment, drugs that improved both parameters were shortlisted as hits for further study. To increase the hit rate, we also identified targets related to chondrocyte phenotype loss according to our previous data (GSE193742) and focused on the drugs regulating relevant pathways in a library containing over 2000 bioactive compounds (Selleck) (Fig. 1D, 1E and Data S1).

After a further 3 rounds of testing, we further trimmed the hit list, and focused on the compound named FPH2 (BRD-9424) (Fig. 1H) which exhibited superior performance (Fig. 1F~1K). FPH2 significantly enhanced chondrocyte phenotype and cell viability (0.5~5μM) (Fig. 1I~1K). 1μM of FPH2 slightly increased the expression of proliferative marker Ki-67 (fig. S1A) and 10μM of the compound was well tolerated in both short-term and long-term culture of human chondrocytes (fig. S1B). These all indicated that FPH2 might act as an suitable compound to boost chondrocyte function and fitness in vitro and in vivo.

FPH2 improved chondrocyte performance in multiple tasks in vitro

To further confirm FPH2's effect, we characterized chondrocyte fitness under different adverse conditions. Primarily, we used hypoxia (5% O_2)-monolayer-cultured P2 chondrocytes (juvenile donors, table S1), the phenotype of which could be easily rescued. After 48 hours, the expression of functional cartilage markers such as collagen type II (COL2) and aggrecan (ACAN) were significantly elevated following FPH2 treatment (fig. S1C). We then tested FPH2's ability to rescue P4 normoxia-monolayer cultured chondrocytes (juvenile donors, table S1) as the function loss was fostered in P4 cells and could be hardly rescued without any intervention *(10)*. Consistently, FPH2 also increased both COL2 and ACAN expression in chondrocytes from murine and human donors (Fig. 2A and 2B). Next, we tested FPH2 performance in more challenging models using continuously normoxia-monolayer cultured human adult chondrocytes (treated from P1 to 4), which were assumed to possess a lower fitness (donors = 7, age 54 ~75y, table S1). Interestingly, it was also shown that FPH2 evidently facilitated their function maintenance, displaying increased ACAN expression in all samples and COL2 expression in 5/7 samples (Fig.

2C, 2D and S1D). These data demonstrated that FPH2 could effectively maintain chondrocyte fitness and phenotype during monolayer passage.

Besides regular culture, we also examined the cell responses to different stimuli. In a redifferentiation induction assay, P4 cell recovery potential was studied in a high density culture model with extracellular matrix (ECM) production as a readout (Fig. 1B, Indicator 3). On this occasion, FPH2-treated P4 chondrocytes were able to form larger matrix-rich micromasses, demonstrating a higher potential of phenotypic recovery (Fig. 2E). The ability of FPH2 to improve ECM production was also validated in the ATDC5 progenitor cell line (fig. S1E), and the effect on cell migration at the edge of micromasses to form larger circles also matched the superior migration in a wound healing assay (Fig. 2F and 2G).

To reveal FPH2's protective function against inflammatory/pathological stimuli, we cultured human cartilage explants with and without the inflammatory factor tumor necrosis factor (TNF)-α (Fig. 2H and 2I). Safranin O and ACAN immunostaining demonstrated that FPH2-treated chondrocytes in the tissues maintained a stronger ability to produce cartilage ECM under stress. In doxorubicin-treated chondrocytes, FPH2 was shown to reduce the development of a senescence-like phenotype (fig. S1F). These all supported that FPH2-treated chondrocytes displayed a higher potential to thrive in adverse conditions and might generate a fitter cell for in vivo regeneration studies.

FPH2-programmed winner cells expressed high levels of fitness-associated genes

Considering the effects on multiple models, we hypothesized that FPH2 might could trigger widely influential programs that boost cell fitness, and cause a change in cell subpopulations via cell competition (occurring when a group of cells gained a higher fitness) *(12, 19)*. To explore this, we used single-cell RNA sequencing (RNA-seq) to detect treated and untreated chondrocytes from both young and adult donors (P3 chondrocytes, donor = 8, fig. S2A and table S1). The data confirmed that the detected 16427 cells preserved their cell identity distinct from that of synovial fibroblasts, although some of them showed a dedifferentiated phenotype after culture, when compared to primary chondrocytes (fig. S2B). The detected cells were generally classified into 8 clusters and 3 subtypes, including a typical chondrocyte cluster (Cluster1, typical chon), energetic clusters (Cluster 3~7) and quiescent clusters (Cluster 0 and 2) (Fig. 3B~3F, Data S2). Typical chon was annotated by gene ontology (GO) terms like *chondrocyte differentiation* and *ECM organization* (fig. S2C). Its proportion was higher in adult compared to young samples, and also

slightly increased in FPH2 groups (Fig.3D and S2A) consistently with the in vitro phenotype tests (Fig. 2A~2D).

Remarkably, we realized a significant change in the proportions of energetic and quiescent clusters, and those clusters showed opposite features. The proportion of energetic clusters increased from 32.8% to 66.7% in young samples and from 29.2% to 61.3% in adult samples, while that of quiescent cells decreased from 66.4% to 24.1% in young samples and from 45.4% to 11.8% in adult samples after FPH2 treatment (Fig. 3D). The quiescent clusters, highly expressed cytoskeletal genes (*ACTG1*, *TMSB10* and *TMSB4X*) but not cartilage lineage markers (Fig. 3E, 3F and S2C), exhibiting a similar phenotype with less-fit dysfunctional chondrocytes according to previous studies *(20, 21)*. On the contrary, the energetic clusters were notably marked by metabolic relevant genes (Fig. 3E), GO terms (*cellular respiration*, *ATP synthesis coupled proton transport*, *aerobic respiration*, and *mitochondrion electron transport*) (Fig. 3F and S2C), and pathways (*oxidative phosphorylation* and *pyruvate metabolism*) (fig. S2D). Moreover, they were not only enriched with metabolic genes but other features, with a dramatic increase in the number of expressed protein-encoding genes compared to the quiescent cells (Fig. 3G). These features were also relevant to cartilage lineage function, protein translation and cell cycle (Fig. 3E). In terms of cell adaptation, genes for sensing and self-regulation were also enriched, including genes related to metabolic stress (*ATF3*) *(22)*, self-checking/protection (*E2F7*, *BCL2L11* and *ATG4D*) *(23-25)* and epigenetic remodeling (*KDM2B* and *KDM3B*) *(26-28)* (Fig. 3G). The signaling for intrinsic self-regulation (*p53 signaling pathway*, *FoxO signaling pathway* and *JAK-STAT signaling pathway*) *(29-32)* was marked in pathway analysis (fig. S2D). In the decipher of cell-cell communication, the interaction strength was shown to be higher between energetic clusters relative to quiescent ones (Fig. 3H and S3A), with a stronger signal of Laminin Subunit Alpha 4 - CD44 that was highly associated with chondrocyte migration and cartilage growth (Fig. S3C~S3E) *(33)*.

Therefore, the data suggested that FPH2 resulted in cell fitness change and increased the proportion of energetic populations. Energetic clusters generally expressed more protein-encoding genes, which were involved in many essential processes and could provide preparation for cell adaptation in various conditions. The increase in expressed gene number in single-cell analysis was in agreement with the increased genes detected by bulk RNA-seq (Fig. 3J). The up-regulated of translation-related genes was also consistent with the elevation of total protein concentration in FPH2-treated cells (Fig. 3K). The broad activation of adaption-responsible genes was paralleled

with the gene expression tendency in real-time qPCR results (fig. S2E). Additionally, the high expression of genes for metabolic processes and homeostasis in energetic clusters, was also consistent with the bulk RNA-seq data showing an up-regulation of genes for glycolysis (*Aldoc*), tricarboxylic acid cycle (*Idh1*), mitochondrion protection (*Vdac2* and *Sod3*) *(34)*, mitochondrial protein translocation (*Timm8a1*, *Timm8b* and *Tomm20*) *(35)* and mitochondrial tRNA processing (*Trnt1* and *Trmt5*) *(36, 37)* in FPH2-treated cells (fig. S4C). This might interpret the findings that FPH2-chondrocytes better fitted in the cultures with an unphysiological oxygen concentration (Fig. 2A~2D). And the cell-cell interaction analysis possibly supported the superior cell migration in wound healing (Fig. 2F and 2G).

Given that fitter cells usually displayed improved protein synthesis, and dysfunctional cells were marked by transcription repression/translation attenuation *(38-40)*, these data supported the finding that FPH2-cells exhibited multiple superiorities in different tasks. FPH2 drove chondrocytes to a winner status, with a highly expression of self-regulatory genes potentially providing "saturated rescue" programs that maintained cell homeostasis in changeable environments (Fig. 3A).

FPH2 inhibited the activity of carnitine palmitoyl transferase I

We then attempted to dissect the specific molecular mechanisms involved in the induction of cell fitness. We employed a prediction tool Similarity Ensemble Approach, to search the possible targets of FPH2 based on chemical similarities between the drug and the ligands of potential targets *(41)*. The top candidates were the isoforms of carnitine palmitoyl transferase I (CPT1A, liver; CPT1B, muscle), rate-limiting enzymes for long-chain fatty acid oxidation (FAO) (Fig. 4A and table S2) *(42)*. Considering the most evident feature in the RNA-seq data, was the high levels of expression of metabolic-related genes, we hypothesized that FPH2's effect might be through the regulation of CPT1 activity, which plays a key role in metabolism (Fig. 4B). Supporting this, both isoforms of CPT1 were found to be expressed in chondrocytes and their inhibition could reduce damage in OA chondrocytes or promote tissue regeneration *(27, 43, 44)*. Besides, their conservation in different species (Fig. 4C) was consistent with the common effect of FPH2 on both human and mouse cells (Fig.1~2).

To validate the effect on CPT1, we detected its activity and function. Using an activity kit, we demonstrated a concentration-dependent suppression of CPT1 activity by FPH2 treatment (0.5~2.5μM) (Fig. 4D). In the examination of CPT1-mediated FAO, we adopted a live-cell oxygen

consumption rate (OCR) assay supplemented with palmitate. The data showed that FPH2 pre-treatment significantly suppressed the level of palmitate OCR with reduced levels of basal respiration, maximal respiration and adenosine triphosphate (ATP) production (Fig. 4E and 4F). These confirmed that FPH2 significantly inhibited the activity of CPT1 and the level of FAO.

A molecular docking analysis was conducted to present the possible drug-target interactions. The highly similar three-dimensional structures of human CPT1A and CPT1B were retrieved (https://alphafold.ebi.ac.uk/) (Fig. 4G). In the docking analysis, FPH2 was displayed to interact with several amino acids of CPT1A/B by hydrogen bonds (Tyr589, A591 and Ser687) and arene-hydrogen interactions (Ser687 and Phe712) respectively (Fig. 4G). Tyr589 was documented as the binding site of (R)-carnitine essential for CPT1 catalysis (https://www.uniprot.org/uniprotkb/P50416/entry; https://www.uniprot.org/uniprotkb/Q92523/entry) *(45)*. Another interacted amino acid Ser687 was predicted to form a conserved motif with Ser685 and Thr686, which contributed to the stabilization for enzyme conformation *(45)*. These supported that FPH2 obstructed the catalytic process of CPT1.

To uncover if FPH2 led to a wide metabolic alteration, we employed untargeted metabolomics. 1917 metabolites were identified and FPH2 samples demonstrated a distinct profiling from control ones, with 118 significantly up- and 400 down-regulated metabolites (Fig. 5A, 5B and Data S3). Consistently, in searching for CPT1-related moderations, we found a reduced accumulation of acyl-carnitines (lauroyl-carnitine and eicosanoyl-carnitine), which belonged to first-step products in CPT1-mediated FAO (fig. S5C) *(46)*. These indicated a suppressed fatty acids catabolism and a potential accumulation of unused lipids. However, we realized an evident down-regulated enrichment of lipid metabolites. Particularly, lipid and lipid-like molecules were the most abundant superclass in the differentially regulated metabolites, and 83.6% of the lipids were down-regulated in FPH2 group (Fig. 5C). A broad inhibition of related pathways was also shown (fig. S5B). The representative down-regulated molecules, which were correlated with fatty acid metabolism, included 8-hydroxyeicosatetraenoic acid (8-HETE, a peroxisome-related fatty acid), (R)-3-Hydroxydodecanoic acid (a medium-chain fatty acid derivative), palmitoyl glycerol (a fatty acid ester) and several acylglycines (N-Decanoylglycine, Tridecanoylglycine, and N-Undecanoylglycine) (Fig. 5D). Taken together, the metabolomics demonstrated a suppression of CPT1 catalysis and an obstruction of lipid metabolism.

In all, we proposed a potential mechanism highly associated with the hinder of CPT1 essential for lipid catabolism. Lipid accumulation was down-regulated, suggesting the existence of other intrinsic compensatory regulation or energy supply pattern, which potentially prevented the accumulation of harmful metabolites.

FPH2 induced an optimal metabolic pattern and boosted energy production

FAO activation produces extra energy for cells under stress, but it does not benefit hypoxic chondrocytes when compared to sugar metabolism, due to the high demand of oxygen and the possible induction of oxidative stress *(47)*. Using a PPAR agonist (GW501516) *(48)*, we confirmed this hypothesis by showing that activation of FAO significantly reduced chondrocyte functional phenotype (fig. S6A and S6B). According to the putative mechanisms, FAO or CPT1 inhibition was connected to a compensatory activation of glucose metabolism *(49, 50)*, suggesting that the action of FPH2 could bring other benefits for chondrocyte fitness.

The metabolomics analysis showed advantageous changes in metabolite components. An up-regulation of two down-stream products of methionine metabolism (methylthioadenosine and spermidine) was detected (Fig. 5D and S5E). Methionine was involved in carnitine synthesis, and its abundance was regulated with the change of free carnitine *(51, 52)*. Thus, the two products' accumulation probably resulted from the interruption of carnitine utilization by CPT1 inhibition. Interestingly, both products were relevant to cell fitness regulation. Methylthioadenosine (intermediate of methionine salvage cycle), was an epigenetic regulator of methylation remodeling, the accumulation of which improved cell fitness reportedly *(53, 54)*. Spermidine, could be synthesized via methionine salvage by-products, and was especially able to promote protein translation *(55, 56)*. Their abundance partially explained the improvement of gene expression and protein synthesis in FPH2-treated cells (Fig. 3J and 3K), although further validation might be required .

Besides amino acids, other sugar-derived metabolites, including fructose 1,6-bisphosphate (a key molecule in glycolysis) and uridine diphosphate N-acetylglucosamine (UDP-GlcNAc, a nucleotide sugar for glycosaminoglycan synthesis) were also enriched in FPH2 group (Fig. 5D and S5D). As glycolysis products were crucial to cartilage ECM construction *(57)*, the findings supported the enhanced chondrocyte phenotype in our previous results (Fig. 2A~2D). Therefore, the clues linking metabolism and cell fitness, indicated the acquirement of a superior pattern shifted from lipid metabolism, which produced favorable metabolites for chondrocyte fitness. More importantly,

the preservation of winner status required a large amount of energy. Given the reduction of lipid metabolism (Fig. 5C, 5D and S5B), and the non-significant changes in most amino acids' enrichment (fig. S5E), we examined sugar catabolism, which is an efficient energy supply compared to lipid metabolism *(44, 47)*.

A significant elevation of ATP and the reduction of malic acid and succinic acid were observed, suggesting the consumption of TCA cycle intermediates for ATP synthesis (Fig. 5D and S5D). To validate this, we examined total ATP levels and found an enhancement in FPH2 treated cells (Fig. 5E). Live-cell bioenergetic measurements demonstrated an activation of both extracellular acidification rate (ECAR) and OCR (Fig. 5G). Particularly, the metabolic rate under basal and stress glycolytic conditions were increased, and the levels of basal respiration, maximal respiration and ATP production in OCR tests were also elevated (Fig. 5I). These verified that FPH2-cells gained an increased level of glucose metabolism to provide essential metabolites and energy for cell fitness, in a more efficient and suitable manner.

Considering the requirement of CPT1 for complete mitochondrial function, we realized that FPH2 was different from the most widely used CPT1 inhibitor Etomoxir (Eto), which irreversibly binds CPT1 and causes mitochondrial toxicity *(58, 59)*. Instead, FPH2's inhibition was relatively moderate, as the drug-target interactions were estimated based on weak bonds (Fig. 4G). With a relatively high dose of FPH2 in cell culture (2.5 μM), the enzyme activity was inhibited no more than 50% (Fig. 4D). Notably, FPH2 increased chondrocyte phenotype and migration, but Eto failed to induced a similar outcome (fig. S7A~S7D). Additionally, FPH2-treated cells contained homogeneous mitochondria with increased mitochondrion membrane potential (MMP) without high levels of reactive oxygen species (ROS) production (Fig. 5F and S8F), which was also matched by greater expression of the antioxidant enzyme superoxide dismutase 3 (SOD3) (fig. S4C, S8D and S8E). These data demonstrated the applicable ability of FPH2 in metabolic regulation, as its treatment did not induce mitochondrial dysfunction or homeostasis failure as Eto's.

Taken together, we demonstrated that FPH2-winner cells adopted a superior metabolic pattern, with an activated production of beneficial metabolites and bioenergy for improving cell fitness (Fig. 5J). Additionally, we observed that FPH2 promoted mitochondrial homeostasis, suggesting that it could serve as an applicable reagent for in vitro cell culture and tissue repair in vivo.

FPH2 improved cell fitness and cartilage regeneration in vivo

Next, we further tested FPH2's role in cartilage repair in vivo. We used FPH2-cultured human chondrocytes in a workflow simulating autologous chondrocyte implantation (ACI) for the treatment of cartilage injuries *(11, 60)* (Fig. 6A). Human adult chondrocytes (n = 6, table S1) were isolated, expanded till P4, and redifferentiated as spherical pellets. FPH2 was used during the whole culture process, and then the expanded pellets were implanted in a full-thickness cartilage defect model of rats.

12 weeks post operation, no hyaline cartilage but only fibrous tissues were shown in the untreated blank group, representing poor repair of the host articular cartilage (Fig. 6B). In the therapeutic groups implanted with control chondrocytes, we only observed a 33% (3/9) probability of forming hyaline cartilage in vivo (Fig. 6B, 6C, and S9B). Notably, after the treatment by FPH2, the chondrocytes from the same resources resulted in an increased regeneration of hyaline cartilage (50%, 4/8), suggesting that FPH2 promoted their potential to maintain lineage phenotype in vivo (Fig. 6B, 6C, and S9B). No tumor-like tissues were seen in those samples (Fig. S9B).

Tissue integration is also an important indicator for cell transplantation and cartilage repair. In our results, untreated chondrocytes hardly integrated with surrounding host tissues, showing unhealed gaps and sharp boundaries (Fig. 6B, yellow arrows), while FPH2-chondrocytes induced an improved tissue integration in the interfaces with a natural-like smooth transition (Fig.6B, black arrows, 6C and S9A).

To confirm the contribution of implanted chondrocytes in repairing tissue interface, we identified human cells with human Lamin A/C antibody. It revealed that FPH2-induced chondrocytes were more capable of migrating, growing into the host cartilage, and forming a larger integrated area with a smooth transition (Fig. 6D and 6E). Whereas, the control group mostly displayed a clear boundary (Fig. 6D and 6E). These matched our in vitro data that FPH2 promoted cell motility (Fig. 2F and 2G), and also suggested that the treatment endowed chondrocytes with a stronger ability to survive and maintain lineage function when growing in vivo.

In additional to chondrocyte implantation, we also examined the function of FPH2 on in situ chondrocytes with a cell-free therapy. We established a control release system of FPH2 by encapsulating it in gelatin microspheres (GM) and incorporating them in a hydrogel suitable to be coated on the joint surfaces (fig. S10A~S10D). A partial-thickness cartilage defect rat model was adopted to mimic an unhealed cartilage injury without bone marrow stem cell repair, which could

possibly lead to further damages like OA *(61)*. FPH2-loaded hydrogel was delivered at the injured surfaces and the FPH2-treated samples were marked by a larger area of COL2-postive cartilage after 8 weeks, while blank and hydrogel control groups were shown with fibrous tissues (fig. S11A and S11B). The newly regenerated cartilage in FPH2 group exhibited typical polygonal/round chondrocytes (fig. S11B). We also observed that FPH2 reduced a cartilage degradative phenotype by measuring the degradation marker matrix metalloproteinase 13 (MMP13) (fig. S11C). The OARSI scoring also indicated an ameliorated potential of early OA onset (fig. S11D). These demonstrated that in situ treatment of FPH2 also positively improved chondrocyte phenotype and cartilage regeneration.

Conclusively, the results confirmed the FPH2's function on chondrocyte fitness by showing promoted cartilage regeneration in animal studies. FPH2-treated human adult chondrocytes obtained a superior fitness to maintain lineage phenotype and integrate well with the host tissues in a cell implantation therapy in cartilage injuries. FPH2-loaded hydrogel also benefited cell fitness in the cartilage niche and prevented OA development at joint surfaces. In all, the data illustrated that FPH2 was able to induce winner chondrocytes with superior metabolic activity and regenerative capacity, suggesting the promise of its future application in human tissue regeneration (Fig. 7).

Discussion

The complete regeneration and repair of tissue is composed of complex numerous cellular tasks, including cell homing, colonization, proliferation, differentiation and stability *(62, 63)*. Cell fitness, the ability of responding and adapting to different signals, plays a key role through all the stages. Therefore, the fabrication of super-fit cell resources is a vital goal in cell therapy and tissue engineering. Although cell fitness has been extensively discussed *(2, 3)*, a convenient, effective, safe and applicable approach for its regulation remains to be developed. Here, this proof-of-concept study demonstrated the possibility of manipulating cell fitness by a single chemical molecule and provided a handy tool to be adopted in cell culture and tissue regeneration. Previously, FPH2 was shown to facilitate functional proliferation of human hepatocytes *(64)*, confirming its positive effect on cell viability and suggesting a potential of multilineage applicability. Importantly, FPH2 exhibited low levels of cytotoxicity (fig. S1B) and did not induce mitochondrial dysfunction (Fig. 5E~5I) nor initiate tumor formation in vivo (fig. S9B). Given that a safe one-fits-all gene editing strategy has not been established, this study provides a cost-effective approach to

optimizing cell fitness for cell therapy and tissue engineering.

In this study, we also introduced new findings to update the concept of cell fitness, by shaping a chemically programmed winner status. Previously, cell survival and growth were the major indicators of fitness, and the trigger of cell competition *(12)*. Although other features, such as protein synthesis or energy metabolism, were also detected, thriving subpopulation growth is the most common phenomenon reported in many cases including those of hepatocytes, cardiomyocytes and neuronal tissues *(4, 65, 66)*. However, gaps still exist between the observation of cell growth and the aim of a complete tissue regeneration. For example, in the pathological analysis of OA, the presence of cell clustering represented a compensatory proliferation of some chondrocytes, but these did not achieve whole tissue function restoration *(67)*, due to the lack of other functional compensation. In this study, we detail additional features that underpin chondrocyte fitness, showing that FPH2 not only facilitated cell proliferation, but also chondrocyte secretory phenotypes (Fig. 2). Besides the cartilage specialized function, our data suggested that FPH2 evidently increased the occupancy of energetic winner subpopulations and decreased that of dysfunctional cells, aligned with the common recognition of cell competition *(19)*. Additionally, we illustrate the superiority of these programmed cells in many other aspects, including their expression of numerous fitness genes, the activation of intercellular interaction (fig. S3C~S3E), and the enhanced migratory behavior (Fig. 2F, 2G, 6D and 6E) that potentially addressed the healing issue at host-implant interfaces *(68)*. These findings propose additional features for determining cell fitness in the context of tissue regeneration, and compelling mechanistic insights that may extend beyond cartilage.

Notably, the winner cells in our study displayed a typically improved metabolism, associated with the chemical modulation of CPT1. Although it is a highly conserved protein essential for cell survival, and a well-known target in many diseases *(27, 42, 43, 47)*, the connection of CPT1 and cell fitness was not established previously. Our findings revealed that FPH2's inhibition of CPT1 triggered a wide range of metabolic alterations and a fine tuning of cellular bioenergetics (Fig. 5, S5 and S8). The treated cells rejected unsuitable metabolic pattern and adopted sugar metabolism with an increase of certain metabolites known to be functional in epigenetic remodeling, protein translation or ECM building (Fig. S5D and S5E). Accumulation of methylthioadenosine was correlated with enhancement of cell fitness and stemness reportedly, as it tended to alter global methylation level, and thereby increased the potential of gene expression with the DNA

hypomethylation state *(53)*. Another product spermidine was an anti-stress polyamine, documented to be important for protein synthesis *(55, 56)*. The findings and connections need further validation, especially in this certain condition and cell type. But it partially explained the potential mechanisms by which FPH2-cells prepared a "saturated rescue" for multiple tasks with more copies of genes and proteins, which were the basis for the high-functioning state, and the strong self-regulatory homeostasis. Taken together, these data demonstrated a novel chemical-induced state with improved cell functionality in vitro and in vivo, which brings a new perspective to the understanding of cell fitness. It also verifies the therapeutic role of CPT1 in tissue regeneration, and proposes a new reagent to modify its activity, in a superior manner to the irreversible inhibitor Eto.

The breakdown of articular cartilage is a world-wide health issue *(9)*. Articular cartilage is shown with a sparse distribution of chondrocytes that only account for 1-5% of the tissue weight *(8)*. Consequently, the empowerment of chondrocyte fitness becomes crucial to cartilage function restoration. It is worth noting that FPH2 significantly improved the therapeutic effect of continuously expanded human adult chondrocytes, and the cells were mostly from aged donors (> 60 year old, tables S1). This is potentially valuable for the future ACI, which is the gold-standard therapy for focal cartilage defects but not recommended for aged patients (> 50 years old) *(69)*. Impressively, FPH2 could also be applied in the treatment of partial-thickness cartilage defect to prevent the development of early OA, which also implied that this compound could be used to directly treat tissue repair or modulate tissue niches for pre-implantation treatment. These together offer a new pharmaceutical therapy effective for cell-based cartilage regeneration. Due to the conservation of target CPT1, the essence of cell fitness in tissue regeneration, and the evidences that FPH2 might function effectively in different cell types *(64)*, FPH2 also holds the potential to be applied to other injuries or degenerative diseases in musculoskeletal systems in the future, such as the treatment for bone fracture or tears in the meniscus.

In summary, this study proposes a chemical tool to manipulate chondrocyte cell fitness and the tissue niche in vivo. The identification of a FPH2-induced winner status and superior performance in tissue regeneration provides attractive prototype therapies for human osteochondral disease in the future.

Materials and Methods

Experimental design

This study was design to identify a small molecule compound that could improve chondrocyte fitness. We adopted a previously established chondrocyte fitness model for drug screening, and then identified a compound named FPH2 that increased both chondrocyte proliferation and lineage phenotype. Next, multiple in vitro tests were conducted to characterize the effect of FPH2 and the results suggested that FPH2 broadly improved cell performance, especially in maintaining chondrocyte phenotype and enhancing migration. To uncover the possible mechanisms, single-cell transcriptomics, target prediction, molecular docking, enzyme activity examination, live-cell bioenergetics measurements, untargeted metabolomics and other functional tests were conducted. For evaluating the in vivo function of FPH2, two rat cartilage injury models were used in animal studies. In a full-thickness cartilage defect model, human chondrocytes were treated with FPH2 and then implanted to heal the defects, the process of which simulated clinical chondrocyte implantation. In another rat model, partial-thickness cartilage defects were created to mimic early-stage cartilage injuries, and were treated with an acellular FPH2-loaded hydrogel. By histological analysis, FPH2 was shown to enhance the formation of hyaline-like cartilage and integration of tissue interfaces. This study was designed for providing an applicable strategy to regulate chondrocyte fitness, and insights into the regulatory mechanisms of cell fitness.

Cell/tissue culture

Cell resources: murine chondrocytes were obtained from the knee joints of postnatal C57Bl/6 mice (postnatal 0-4 days) based on a previously published protocol *(70)*. Human young chondrocytes were collected from embryonic cartilage or infant polydactyly tissues following an established protocol (table S1, n = 9, age 17w~1y) *(71)*. Human adult chondrocytes were harvested from knee cartilage of OA patients after joint replacement surgeries or macroscopically normal cartilage from patients with traumatic cartilage injury (table S1, n = 15, age 23y~76y). The use of human tissues in this study was approved by the Institutional Review Board/Ethics Committee of Children's hospital of Zhejiang University (2020-IRB-007), the Ethics Committee of the First Affiliated Hospital of Zhejiang University (2018-115), the Ethics Committee of the Fourth Affiliated Hospital of Zhejiang University (K2021088). All the human tissues were collected after the donors (or their legal guardians) signed informed consent documents.

For chondrocyte isolation, cartilage tissues were washed in phosphate buffered saline (PBS), cut into 1 mm^3 slices and digested with 0.2% collagenase type II (Gibco) at 37 °C. For embryonic and

infant tissues, the digestion took 6~8 hours, while for adult tissues the digestion time could be optimized to 16 hours. 0.1% collagenase type I (Gibco) could be optionally added in the medium to accelerate the digestion. On the next day, the solution was filtered by a 40 μm filter and the cells were collected by centrifugation at 1200~1700 rpm for 5 min. Then the chondrocytes could be cultured in DMEM/F12 medium (Gibco) with 10% serum at 37 °C with 5% CO_2.

For cell/tissue treatment, FPH2 was dissolved in dimethyl sulfoxide (DMSO) and further diluted in culture medium. Same amount of DMSO was added in control groups. The concentration of FPH2 (0.5~2.5 μM) used in different experiments are detailed in the figures or figure legends. FAO agonist GW501516 and CPT1 irreversible inhibitor Eto were used at a concentration of 1 μM and 2 μM respectively. For monolayer culture, chondrocytes were passaged based on the doubling of cell population on Petri dishes in normoxia (21 O_2) or hypoxia (5% O_2). For redifferentiation assay, chondrocytes were centrifuged into high-density cell suspension (10^5 cells in 10 μl medium), and placed into 24-well culture plates. The cells were incubated for 4 hours to form micromasses. Then growth medium was added gently without spreading the cells. After 48 hours, micromasses were fixed using 4% paraformaldehyde (PFA) and stained by alcian blue (scytek). For wound healing assay, human chondrocytes were cultured in dishes until 95~100% confluency. Cell-free gaps were created by a pipette tip and the floating cells were washed away by changing the culture medium with serum-free FPH2-containing medium. Then the cells were imaged by a light microscope. After 16 hours (overnight), the cells were rinsed and imaged by the microscope again. The images at the identical locations (before and after the incubation) were compared and the migratory cells were calculated. For explant culture, cartilage tissues (5mm×1cm×5mm) were cultured in serum-free DMEM/F12 for 24 hours and then treated by 1 μM FPH2 with or without 10 ng/ml TNFα. After 21 days, the tissues were fixed and characterized by histological analysis. Adjacent tissues were compared in pairs based on the intensity of safranin O staining.

Drug screening

Reporter chondrocytes were collected from the knee cartilage of Col2-pd2EGFP transgenic mice gifted by Prof. William A. Horton *(18)*. These cells capture the real-time expression of cartilage functional marker *Col2a1*. In a library containing 2178 chemical compounds (Selleck, Data S1), we narrowed down the range of screen by selecting 289 drugs that facilitated pathways associated with chondrocyte dedifferentiation according to our published scRNA-seq data (GSE193742). These candidate drugs (1 μM) were used to treat P2 reporter chondrocytes in 96-well plates for 48

hours. Then the GFP signaling and cell number were detected with a high-throughput/content imaging system (YOKOGAWA CQ1). Drugs promoting both *Col2a1* expression and cell growth were selected as candidates. DMSO was used as the negative control.

Drug target prediction and molecular docking

The prediction of FPH2 target was made by Similarity ensemble approach server (https://sea16.docking.org/) based on a standard protocol, which relates proteins based on the chemical similarity (table S2). In the molecular docking analysis, the three dimensional structures of human CPT1A/B were retrieved from Alphafold database (https://alphafold.ebi.ac.uk/) and optimized by MOE plugin "Quickprep". In the docking process, MOE plugin "Dock" was employed, and the fast Fourier transform was used to search the interaction mode. CPT1 proteins were coarse-grained. The coarse-grained model and the side chain of contact residues were optimized, retaining up to 1000 conformations by London δ score function. Next the docking poses were further optimized by energy minimization, and the binding energies were calculated by GB/VI scoring function. The top 100 poses were retained and clustered to select the best one as the final outcome.

Extracellular flux analysis, CPT1 activity assay and mitochondrial functional test

In the extracellular flux assay for live-cell bioenergetics, Seahorse XF Glycolysis Stress Kit, Cell Mito Stress Test Kit, and Palmitate Oxidation Stress Test Kit were utilized to a Seahorse XF96 extracellular flux analyzer (Agilent). In ECAR and OCR assays, P4 chondrocytes (pretreated with 1μM FPH2 for 48 hours) were seeded in XF96 microplates (12,000/well) and cultured overnight. The cells were equilibrated for 1 hour before the assays. Following the standard programs, compounds were injected at the following order and final concentrations: 10mM glucose, 1μM oligomycin and 50 mM 2-2-deoxyglucose (2-DG) for the ECAR assay; 1.5 μM oligomycin, 1 μM FCCP and 0.5 μM Rotenone/Antimycin A for the OCR assay. For palmitate OCR assay, chondrocytes (pre-treated with 1μM FPH2 for 48 hours) were seeded at a density of 10,000/well and cultured overnight. One day prior to the assay, the seeded chondrocytes were treated with substrate-limited growth media (0.5 mM glucose, 1 mM glutamine, 1% serum and 0.5mM L-carnitine). On the day of assay, the medium was changed into test assay media (2 mM glucose and 0.5 mM L-carnitine) for an 1 hour-equilibration. Following the standard protocol, palmitate-bovine serum albumin (BSA) (30μl per well) was added into the wells just prior to starting the assay and compounds were injected at the following order and final concentrations during the test program:

assay medium, 1.5 μM oligomycin, 2 μM FCCP and 0.5 μM Rotenone/Antimycin A. The outcomes were analyzed based on the standard templates.

For CPT1 function detection, a CPT1 activity assay Kit (Suzhou Comin Biotechnology Company) was adopted. Whole-cell lysates were mixed with reaction buffer (1~2 mM ethylenediaminetetraacetic acid (EDTA), 200 μM 5,5′-dithiobis-(2-nitrobenzoic acid) (DTNB), and 80 μM palmitoyl-CoA) and incubated for 5 min at 37 °C. After L-carnitine was added in the reaction, a photometric measurement at 412 nm was immediately conducted. The final outcomes of CPT1 activity were normalized by the protein concentration in each sample.

In the mitochondrial function test, the levels of ATP, mitochondrial membrane potential (MMP), and reactive oxygen species (ROS) were measured using an Enhanced ATP Assay Kit (Beyotime), an Enhanced mitochondrial membrane potential assay kit with JC-1 (Beyotime) and a Reactive Oxygen Species Assay Kit (Beyotime) respectively following manufacturer's instructions. The morphology of mitochondria were marked with the staining of MitoTracker™ Red CMXRos (ThermoFisher) under a confocal microscope.

Single-cell transcriptomics

Human infant (n = 4) and adult (n = 4) chondrocytes (P3, table S1) were cultured in FPH2-containing medium for 48 hours and then detached as a single-cell suspension. Then suspension was processed based on the standard protocol of micro-well single-cell RNA-seq *(72)*. Briefly, in micro-well plates, digested cell suspension (cell concentration: 100,000/ml) was loaded onto barcoded beads on a magnet and then incubated with cold lysis buffer. The beads were collected, washed, and incubated with reverse transcription mix (Takara). In cDNA library preparation, the beads were processed in PCR procedures (Kapa Biosystems) and then the supernatant were pooled and purified (Vazyme). Next, using a customized transposase, the purified cDNA libraries were fragmented following standard instructions. The samples were subjected to sequencing on the Illumina HiSeq with our custom R1 sequencing primers to ensure the completion of the sequencing.

In the single-cell transcriptomics analysis, the raw reads were aligned to the human reference genome (GRCh38) by BBMap (v35.85) and Drop-seq_tools (v1.12). The mixed-genotype single-cell RNA sequencing experiments clustered by individual using souporcell (v2.4) *(73)*. Subsequently, the single cells and their UMI count matrices were imported into the python package Scanpy (v1.9.1) for further analysis *(74)*. Briefly, cells were filtered to include at least 200 genes present in each cell and a minimum of three cells were discarded (min_cells = 3, min_features =

200, percent.mt < 35). The gene expression measurements for each cell were normalized with a scale factor of 10000, and top 2000 variable genes were calculated. Then Principal Component Analysis (PCA) was performed (n_pcs = 30), followed by Uniform Manifold Approximation and Projection (UMAP) analysis (reduction = "pca", dims = 1:30). Cell-cell communication analysis was carried out using the R package CellChat v1.5.0 to compare multiple datasets with distinct cell type compositions *(75)*.

Raw sequence data was deposited in the Genome Sequence Archive in National Genomics Data Center, China National Center for Bioinformation/Beijing Institute of Genomics, Chinese Academy of Sciences (GSA-Human: HRA006517) (https://ngdc.cncb.ac.cn/gsa-human) *(76, 77)*.

Untargeted metabolomics

2×10^7 SW1353 cells were treated by 2.5 μM FPH2 or 0.005% DMSO (n = 4 for each group) for 48 hours. Then they were detached by a scraper, and collected by centrifugation (1800 rpm, 4 °C, 10 min). The metabolites were extracted with 1ml precooled methanol/acetonitrile/water (v/v, 2:2:1) under sonication for 1 hour on ice. The mixture was incubated at -20 °C for 1 hour followed by centrifugation at 14,000 g, 4 °C for 20 min. Dried extracts were then dissolved in 50% acetonitrile, filtered with a disposable 0.22 μm cellulose acetate, and stored at -80°C.

Metabolomics profiling was analyzed with a UPLC-ESI-Q-Orbitrap-MS system (UHPLC, Shimadzu Nexera X2 LC-30AD) coupled with Q-Exactive Plus (Thermo Scientific). The samples were detected with a ACQUITY UPLC® HSS T3 column (2.1×100 mm, 1.8μm). The flow rate was 0.3 ml/min and the mobile phase contained: A: 0.1% FA in water and B: 100% acetonitrile. The gradient was 0% buffer B for 2 min with a linear increase to 48% in 4 min, and then it was up to 100% in 4 min, maintained for 2 min, and down to 0% buffer B in 0.1 min, with 3 min re-equilibration period employed. Quality control samples were prepared by pooling all samples and used for data normalization. Blank samples (75 % acetonitrile in water) and quality controls were injected every six samples during acquisition. The raw data were processed using MS-DIAL for peak alignment, retention time correction and peak area extraction. The metabolites were identified by accuracy mass (mass tolerance < 10 ppm) and MS/MS data (mass tolerance < 0.02 Da), and were matched with HMDB, massbank, and our self-built library. Variables having over 50% of the nonzero values in at least one group were kept in the extracted-ion features.

For data analysis, R(4.0.3) and its packages were used. Models were built on principal component analysis (PCA), and orthogonal partial least-square discriminant analysis (OPLS-DA). The

variable importance on projection (VIP) scores indicated the variables' contribution to the discrimination between all the classes of samples. Metabolites with VIP values greater than 1.0 and *p* values less than 0.05 were considered to be statistically significant metabolites. Fold change was calculated as the logarithm of the average mass response (area) ratio between two arbitrary classes. The identified metabolites were used to perform biological pathway analysis using KEGG database (http://www.kegg.jp).

Immunostaining

In the immunofluorescence staining, cells seeded on coverslips were fixed by 4% PFA for 20 min. Prepared tissue sections were subjected to the processes of deparaffinization, hydration and antigen retrieval processes. Then they were incubated in 0.03% Triton X-100 followed by a BSA blocking for 1h at room temperature (RT). Then the samples were incubated with certain primary antibodies overnight (~16 hours) at 4°C, and then treated with appropriate secondary antibodies for 3 hours at RT.

For immunohistochemistry staining, rat or human cartilage sections were processed according to standard protocols, including antigen retrieval, inactivation of endogenous peroxidase, BSA blocking, incubation of primary antibodies and proper secondary antibody (Beyotime). The stained specimens were photographed under a Digital Slide Scanner (3D Histech).

The primary antibodies included: COL2 antibody (Novusbio, NB600-844), ACAN antibody (Abcam, ab3778, ab36861), Ki67 antibody (Abcam, ab16667), MMP13 antibody (Abcam, ab39012), Lamin A/C antibody (Abcam, ab108595), COL1 antibody (Novus, NB600-408), and ALexar Fluor 546 phalloidin (1:50, Invirogen, A22283).

Pharmaceutical hydrogel preparation

FPH2-loaded gelatin microspheres (GM) were prepared as previously described *(78)*. 15 mg FPH2 was mixed with 600 μl gelatin solution (250 mg/ml). The mixture was then added dropwise into 3 ml liquid paraffin with 50 ul Span 80 at 50 °C, with constant stirring at 600 rpm for 15 min. Next the emulsion was cooled on ice with constant stirring for 30 min and added with 1 ml glutaraldehyde for crosslinking. After a continual stirring of 2 hours, 2 ml acetone was added. Then we collected the supernatant and added 1 ml acetone before the overnight solidifying. The FPH2-GMs were washed, vacuum free-dried, and stored for further utilization. For the preparation of joint adhesive hydrogel, gelatin methacrylate (GelMA), *N*-(2-aminoethyl)−4-(4-(hydroxymethyl)−2-methoxy-5-nitrosophenoxy) butanamide (NB) linked to the

glycosaminoglycan hyaluronic acid (HA-NB), and the photo-initiator lithium phenyl-2,4,6-trimethylbenzoylphosphinate (LAP) were synthesized based on the previous method *(79)*. Briefly, for GelMA synthesis, type A gelatin (Sigma-Aldrich) was added into PBS (10% w/v) and stirred at 50 °C. After the formation of a homogeneous solution, methacrylic anhydride (MA) (Sigma-Aldrich) (0.1 ml per g of gelatin) was slowly added with continuous stirring. Then, the mixture was incubated at 50 °C for 3 hours. The solution was next dialyzed using 8-14 kDa cutoff against deionized water for 7 days at 50 °C. The product was frozen overnight and then lyophilized. For HA-NB synthesis, HA (408 mg, Dongyuan Biotech) was dissolved in 50 ml deionized water. NB (224 mg, synthesized by previously methods *(79)*) and hydroxybenzotriazole (HOBt) (153 mg, Sigma-Aldrich). After pH adjustment (to 4.5), 1-(3-Dimethylaminopropyl)-3-ethylcarbodimide hydrochloride (200 mg, 1.04, Sigma-Aldrich) were suppled into the mixture, which was stirred for 48 hours at RT. The solution was dialyzed (molecular weight cut off 3500) against diluted HCl (0.1 M NaCl, pH 3.5) for 2 days, dialyzed against deionized water for 2 days, and then lyophilized for further uses. For preparation of adhesive hydrogel, the free-dried FPH2-GMs, GelMA foams, and HA-NB foams were dissolved in PBS at 45 °C at the following final concentration: 250 μM FPH2, 5% GelMA and 1.25% HA-NB. 0.25% LAP was mixed in hydrogel solution just after the establishment of partial-thickness cartilage defect model in the animal study. Then the solution was painted to cover the defects, and exposed to UV light (365 nm, 30 mW/cm^2, for 20s) for cross-linking.

Animal study

The use of murine chondrocytes and the conduction of in vivo study was approved by the Zhejiang University Ethics Committee (ZJU20200032). For the full-thickness cartilage defect model, human chondrocytes from 6 adults were used to be implanted into the joints of Sprague–Dawley (SD) rats. Briefly, human chondrocytes isolated from macroscopically normal knee cartilage of OA patients were expanded on petri-dishes until P4, and then formed chondrogenic pellets (3×10^5 cells per pellet) in a suspension culture for 7 days. 1 μM FPH2 or 0.002% DMSO were continuously used in the culture medium. In the joints of 10-week-old male SD rats, cylindrical defects (diameter: 1.5 mm; depth: 2 mm) were created on the trochlear groove of the femurs by a drill bit. The defects were left untreated (blank group, n = 8), implanted with FPH2-treated chondrocyte pellets (hchon-FPH2 group, n = 8) or implanted with DMSO control pellets (hchon-Ctrl, n = 9). Samples in sham group served as healthy controls (n = 4). Based on the previously

established protocol, the rats were orally administrated with cyclophosphamide (4 mg/kg/d ENDOXAN) to suppress the immune responses to human implants. 12 weeks after the surgery, rat were sacrificed and the joints were collected for histological analysis and scoring.

For partial-thickness model, 10-week old male SD rats were anesthetized and their joint cavities were exposed for creating partial thickness defects (size: 2mm × 2mm; depth: 0.2 mm) on the femoral trochlear groove with a custom-made scalpel. FPH2-loaded hydrogel was adhered to the defects by cross-linking under UV light. Sham group, untreated defect group and FPH2-free hydrogel group were used as controls (n=6 for each group). 8 weeks after the surgery, knee joints were harvested for histological analysis. Joint samples were fixed and decalcified in neutral 10% EDTA solution. They were subsequently dehydrated through an alcohol gradient and embedded in paraffin blocks. Histological sections (7 μm) were prepared using a microtome (Leica), and then stained with fast-green (Sigma) / Safrannin O (Sigma). The representative sections were scored based on a blind scoring using parameters in ICRS-II and OARSI assessment *(7, 80)*.

Statistical Analysis

Two-sided p-value less than 0.05 was considered as the threshold for statistical significance (*p < 0.05; **p < 0.01; ***p < 0.001). Statistical analysis was performed by GraphPad Prism 8. Student's t test was adopted in the comparisons for the data of two groups. For multiple group comparisons, one-way analysis of variance (ANOVA) test with Tukey was used to compare all pairs of groups, and Dunnett test was used to compare control group with the others. Kruskal-Wallis test with Tukey was used for nonparametric analysis.

References

1. W. A. Lim, The emerging era of cell engineering: Harnessing the modularity of cells to program complex biological function. *Science* **378**, 848-852 (2022).
2. L. Shen, Y. Xiao, J. Tian, Z. Lu, Remodeling metabolic fitness: Strategies for improving the efficacy of chimeric antigen receptor T cell therapy. *Cancer Lett.* **529**, 139-152 (2022).
3. N. Shakiba, P. W. Zandstra, Engineering cell fitness: lessons for regenerative medicine. *Curr. Opin. Biotechnol.* **47**, 7-15 (2017).
4. C. Villa Del Campo, C. Clavería, R. Sierra, M. Torres, Cell competition promotes phenotypically silent cardiomyocyte replacement in the mammalian heart. *Cell Rep* **8**, 1741-1751 (2014).
5. J. P. Vincent, A. G. Fletcher, L. A. Baena-Lopez, Mechanisms and mechanics of cell competition in epithelia. *Nat. Rev. Mol. Cell Biol.* **14**, 581-591 (2013).
6. W. Kim, R. Jain, Picking Winners and Losers: Cell Competition in Tissue Development and Homeostasis. *Trends Genet.* **36**, 490-498 (2020).
7. K. P. Pritzker, S. Gay, S. A. Jimenez, K. Ostergaard, J. P. Pelletier, P. A. Revell, D. Salter, W. B. van den Berg, Osteoarthritis cartilage histopathology: grading and staging. *Osteoarthr. Cartil.* **14**, 13-29 (2006).
8. D. J. Huey, J. C. Hu, K. A. Athanasiou, Unlike bone, cartilage regeneration remains elusive. *Science* **338**, 917-921 (2012).
9. D. J. Hunter, L. March, M. Chew, Osteoarthritis in 2020 and beyond: a Lancet Commission. *Lancet* **396**, 1711-1712 (2020).
10. Y. Chen, Y. Yu, Y. Wen, J. Chen, J. Lin, Z. Sheng, W. Zhou, H. Sun, C. An, J. Chen, W. Wu, C. Teng, W. Wei, H. Ouyang, A high-resolution route map reveals distinct stages of chondrocyte dedifferentiation for cartilage regeneration. *Bone Res* **10**, 38 (2022).

11. R. L. Davies, N. J. Kuiper, Regenerative Medicine: A Review of the Evolution of Autologous Chondrocyte Implantation (ACI) Therapy. *Bioengineering (Basel)* **6**, 22 (2019).
12. A. Di Gregorio, S. Bowling, T. A. Rodriguez, Cell Competition and Its Role in the Regulation of Cell Fitness from Development to Cancer. *Dev. Cell* **38**, 621-634 (2016).
13. Y. He, Z. Ji, Y. Gong, L. Fan, P. Xu, X. Chen, J. Miao, K. Zhang, W. Zhang, P. Ma, H. Zhao, C. Cheng, D. Wang, J. Wang, N. Jing, K. Liu, P. Zhang, B. Dong, G. Zhuang, Y. Fu, W. Xue, W. Q. Gao, H. H. Zhu, Numb/Parkin-directed mitochondrial fitness governs cancer cell fate via metabolic regulation of histone lactylation. *Cell Rep* **42**, 112033 (2023).
14. L. S. Lenz, J. L. Faccioni, P. A. Bracco, J. Santos, L. C. Pereira, J. H. Buss, M. T. Tamborindeguy, D. Torgo, T. Monteiro, G. B. Mantovani, C. N. Santo, J. C. Marcolin, E. Dalsin, A. Vigo, S. M. Callegari-Jacques, A. O. Silva, G. R. Onzi, K. R. Begnini, G. Lenz, Cancer Cell Fitness Is Dynamic. *Cancer Res.* **81**, 1040-1051 (2021).
15. J. Wang, S. Sun, H. Deng, Chemical reprogramming for cell fate manipulation: Methods, applications, and perspectives. *Cell Stem Cell* **30**, 1130-1147 (2023).
16. J. Guan, G. Wang, J. Wang, Z. Zhang, Y. Fu, L. Cheng, G. Meng, Y. Lyu, J. Zhu, Y. Li, Y. Wang, S. Liuyang, B. Liu, Z. Yang, H. He, X. Zhong, Q. Chen, X. Zhang, S. Sun, W. Lai, Y. Shi, L. Liu, L. Wang, C. Li, S. Lu, H. Deng, Chemical reprogramming of human somatic cells to pluripotent stem cells. *Nature* **605**, 325-331 (2022).
17. Y. Du, Z. Liang, S. Wang, D. Sun, X. Wang, S. Y. Liew, S. Lu, S. Wu, Y. Jiang, Y. Wang, B. Zhang, W. Yu, Z. Lu, Y. Pu, Y. Zhang, H. Long, S. Xiao, R. Liang, Z. Zhang, J. Guan, J. Wang, H. Ren, Y. Wei, J. Zhao, S. Sun, T. Liu, G. Meng, L. Wang, J. Gu, T. Wang, Y. Liu, C. Li, C. Tang, Z. Shen, X. Peng, H. Deng, Human pluripotent stem-cell-derived islets ameliorate diabetes in non-human primates. *Nat. Med.* **28**, 272-282 (2022).
18. M. A. Tryfonidou, G. P. Lunstrum, K. Hendriks, F. M. Riemers, R. Wubbolts, H. A. Hazewinkel, C. R. Degnin, W. A. Horton, Novel type II collagen reporter mice: New tool for assessing collagen 2α1 expression in vivo and in vitro. *Dev. Dyn.* **240**, 663-673 (2011).
19. K. Lawlor, S. Pérez-Montero, A. Lima, T. A. Rodríguez, Transcriptional versus metabolic control of cell fitness during cell competition. *Semin. Cancer Biol.* **63**, 36-43 (2020).
20. J. C. Lauer, M. Selig, M. L. Hart, B. Kurz, B. Rolauffs, Articular Chondrocyte Phenotype Regulation through the Cytoskeleton and the Signaling Processes That Originate from or Converge on the Cytoskeleton: Towards a Novel Understanding of the Intersection between Actin Dynamics and Chondrogenic Function. *Int J Mol Sci* **22**, 3279 (2021).
21. J. Parreno, M. Nabavi Niaki, K. Andrejevic, A. Jiang, P. H. Wu, R. A. Kandel, Interplay between cytoskeletal polymerization and the chondrogenic phenotype in chondrocytes passaged in monolayer culture. *J. Anat.* **230**, 234-248 (2017).
22. H. C. Ku, C. F. Cheng, Master Regulator Activating Transcription Factor 3 (ATF3) in Metabolic Homeostasis and Cancer. *Front Endocrinol (Lausanne)* **11**, 556 (2020).
23. S. Luo, D. C. Rubinsztein, BCL2L11/BIM: a novel molecular link between autophagy and apoptosis. *Autophagy* **9**, 104-105 (2013).
24. Y. Wang, X. Pei, P. Xu, Z. Tan, Z. Zhu, G. Zhang, Z. Jiang, Z. Deng, E2F7, regulated by miR-30c, inhibits apoptosis and promotes cell cycle of prostate cancer cells. *Oncol. Rep.* **44**, 849-862 (2020).
25. X. Chen, Y. Zhang, Y. Shi, H. Lian, H. Tu, S. Han, J. Yin, B. Peng, B. Zhou, X. He, W. Liu, MiR-129 triggers autophagic flux by regulating a novel Notch-1/ E2F7/Beclin-1 axis to impair the viability of human malignant glioma cells. *Oncotarget* **7**, 9222-9235 (2016).
26. C. Zhang, X. Han, Y. Liang, H. Liu, Z. Fan, J. Zhang, The Histone Demethylase KDM3B Promotes Osteo-/Odontogenic Differentiation, Cell Proliferation, and Migration Potential of Stem Cells from the Apical Papilla. *Stem Cells Int* **2020**, 8881021 (2020).
27. X. Li, F. Wu, S. Günther, M. Looso, C. Kuenne, T. Zhang, M. Wiesnet, S. Klatt, S. Zukunft, I. Fleming, G. Poschet, A. Wietelmann, A. Atzberger, M. Potente, X. Yuan, T. Braun, Inhibition of fatty acid oxidation enables heart regeneration in adult mice. *Nature* **622**, 619-626 (2023).
28. I. Gažová, A. Lengeling, K. M. Summers, Lysine demethylases KDM6A and UTY: The X and Y of histone demethylation. *Mol. Genet. Metab.* **127**, 31-44 (2019).
29. C. de la Cova, N. Senoo-Matsuda, M. Ziosi, D. C. Wu, P. Bellosta, C. M. Quinzii, L. A. Johnston, Supercompetitor status of Drosophila Myc cells requires p53 as a fitness sensor to reprogram metabolism and promote viability. *Cell Metab.* **19**, 470-483 (2014).
30. R. H. Newton, S. Shrestha, J. M. Sullivan, K. B. Yates, E. B. Compeer, N. Ron-Harel, B. R. Blazar, S. J. Bensinger, W. N. Haining, M. L. Dustin, D. J. Campbell, H. Chi, L. A. Turka, Maintenance of CD4 T cell fitness through regulation of Foxo1. *Nat. Immunol.* **19**, 838-848 (2018).
31. K. L. Owen, N. K. Brockwell, B. S. Parker, JAK-STAT Signaling: A Double-Edged Sword of Immune Regulation and Cancer Progression. *Cancers (Basel)* **11**, 2002 (2019).
32. R. Scherz-Shouval, H. Weidberg, C. Gonen, S. Wilder, Z. Elazar, M. Oren, p53-dependent regulation of autophagy protein LC3 supports cancer cell survival under prolonged starvation. *Proc. Natl. Acad. Sci. U.S.A.* **107**, 18511-18516 (2010).
33. F. C. Moazedi-Fuerst, G. Gruber, M. H. Stradner, D. Guidolin, J. C. Jones, K. Bodo, K. Wagner, D. Peischler, V. Krischan, J. Weber, P. Sadoghi, M. Glehr, A. Leithner, W. B. Graninger, Effect of Laminin-A4 inhibition on cluster formation of human osteoarthritic chondrocytes. *J. Orthop. Res.* **34**, 419-426 (2016).
34. E. H. Cheng, T. V. Sheiko, J. K. Fisher, W. J. Craigen, S. J. Korsmeyer, VDAC2 inhibits BAK activation and mitochondrial apoptosis. *Science* **301**, 513-517 (2003).

35. A. M. Sokol, M. E. Sztolsztener, M. Wasilewski, E. Heinz, A. Chacinska, Mitochondrial protein translocases for survival and wellbeing. *FEBS Lett.* **588**, 2484-2495 (2014).
36. Y. Wedatilake, R. Niazi, E. Fassone, C. A. Powell, S. Pearce, V. Plagnol, J. W. Saldanha, R. Kleta, W. K. Chong, E. Footitt, P. B. Mills, J. W. Taanman, M. Minczuk, P. T. Clayton, S. Rahman, TRNT1 deficiency: clinical, biochemical and molecular genetic features. *Orphanet J Rare Dis* **11**, 90 (2016).
37. C. A. Powell, R. Kopajtich, A. R. D'Souza, J. Rorbach, L. S. Kremer, R. A. Husain, C. Dallabona, C. Donnini, C. L. Alston, H. Griffin, A. Pyle, P. F. Chinnery, T. M. Strom, T. Meitinger, R. J. Rodenburg, G. Schottmann, M. Schuelke, N. Romain, R. G. Haller, I. Ferrero, T. B. Haack, R. W. Taylor, H. Prokisch, M. Minczuk, TRMT5 Mutations Cause a Defect in Post-transcriptional Modification of Mitochondrial tRNA Associated with Multiple Respiratory-Chain Deficiencies. *Am. J. Hum. Genet.* **97**, 319-328 (2015).
38. L. Duan, Y. Liang, B. Ma, D. Wang, W. Liu, J. Huang, J. Xiong, L. Peng, J. Chen, W. Zhu, D. Wang, DNA Methylation Profiling in Chondrocyte Dedifferentiation In Vitro. *J. Cell. Physiol.* **232**, 1708-1716 (2017).
39. S. van Erp, A. A. van Berkel, E. M. Feenstra, P. K. Sahoo, L. J. Wagstaff, J. L. Twiss, J. W. Fawcett, R. Eva, C. Ffrench-Constant, Age-related loss of axonal regeneration is reflected by the level of local translation. *Exp. Neurol.* **339**, 113594 (2021).
40. M. Buszczak, R. A. Signer, S. J. Morrison, Cellular differences in protein synthesis regulate tissue homeostasis. *Cell* **159**, 242-251 (2014).
41. M. J. Keiser, B. L. Roth, B. N. Armbruster, P. Ernsberger, J. J. Irwin, B. K. Shoichet, Relating protein pharmacology by ligand chemistry. *Nat. Biotechnol.* **25**, 197-206 (2007).
42. I. R. Schlaepfer, M. Joshi, CPT1A-mediated Fat Oxidation, Mechanisms, and Therapeutic Potential. *Endocrinology* **161**, bqz046 [pii] (2020).
43. N. Jiang, B. Xing, R. Peng, J. Shang, B. Wu, P. Xiao, S. Lin, X. Xu, H. Lu, Inhibition of Cpt1a alleviates oxidative stress-induced chondrocyte senescence via regulating mitochondrial dysfunction and activating mitophagy. *Mech. Ageing Dev.* **205**, 111688 (2022).
44. S. M. Ceccarelli, O. Chomienne, M. Gubler, A. Arduini, Carnitine palmitoyltransferase (CPT) modulators: a medicinal chemistry perspective on 35 years of research. *J. Med. Chem.* **54**, 3109-3152 (2011).
45. M. Morillas, E. López-Viñas, A. Valencia, D. Serra, P. Gómez-Puertas, F. G. Hegardt, G. Asins, Structural model of carnitine palmitoyltransferase I based on the carnitine acetyltransferase crystal. *Biochem. J.* **379**, 777-784 (2004).
46. M. Melone, A. Valentino, S. Margarucci, U. Galderisi, A. Giordano, G. Peluso, The carnitine system and cancer metabolic plasticity. *Cell Death Dis* **9**, 228 (2018).
47. S. C. Hendrickson, J. D. St Louis, J. E. Lowe, S. Abdel-aleem, Free fatty acid metabolism during myocardial ischemia and reperfusion. *Mol. Cell. Biochem.* **166**, 85-94 (1997).
48. M. Idrees, L. Xu, M. El Sheikh, T. Sidrat, S. H. Song, M. D. Joo, K. L. Lee, I. K. Kong, The PPARδ Agonist GW501516 Improves Lipolytic/Lipogenic Balance through CPT1 and PEPCK during the Development of Pre-Implantation Bovine Embryos. *Int J Mol Sci* **20**, 6066 (2019).
49. S. J. Manley, A. A. Olou, J. L. Jack, M. T. Ruckert, R. M. Walsh, A. E. Eades, B. A. Bye, J. Ambrose, F. Messaggio, S. Anant, M. N. VanSaun, Synthetic adiponectin-receptor agonist, AdipoRon, induces glycolytic dependence in pancreatic cancer cells. *Cell Death Dis* **13**, 114 (2022).
50. A. Dalmao-Fernández, J. Lund, T. Hermida-Gómez, M. E. Vazquez-Mosquera, I. Rego-Pérez, F. J. Blanco, M. Fernández-Moreno, Impaired Metabolic Flexibility in the Osteoarthritis Process: A Study on Transmitochondrial Cybrids. *Cells* **9**, 809 (2020).
51. Y. Martínez, X. Li, G. Liu, P. Bin, W. Yan, D. Más, M. Valdivié, C. A. Hu, W. Ren, Y. Yin, The role of methionine on metabolism, oxidative stress, and diseases. *Amino Acids* **49**, 2091-2098 (2017).
52. J. Pekala, B. Patkowska-Sokoła, R. Bodkowski, D. Jamroz, P. Nowakowski, S. Lochyński, T. Librowski, L-carnitine--metabolic functions and meaning in humans life. *Curr. Drug Metab.* **12**, 667-678 (2011).
53. N. Fan, Y. Zhang, S. Zou, Methylthioadenosine phosphorylase deficiency in tumors: A compelling therapeutic target. *Front Cell Dev Biol* **11**, 1173356 (2023).
54. W. Ding, D. P. Higgins, D. K. Yadav, A. A. Godbole, R. Pukkila-Worley, A. K. Walker, Stress-responsive and metabolic gene regulation are altered in low S-adenosylmethionine. *PLoS Genet.* **14**, e1007812 (2018).
55. T. E. Dever, I. P. Ivanov, Roles of polyamines in translation. *JOURNAL OF BIOLOGICAL CHEMISTRY* **293**, 18719-18729 (2018).
56. F. Madeo, T. Eisenberg, F. Pietrocola, G. Kroemer, Spermidine in health and disease. *Science* **359**, eaan2788 [pii] (2018).
57. A. Mobasheri, S. J. Vannucci, C. A. Bondy, S. D. Carter, J. F. Innes, M. F. Arteaga, E. Trujillo, I. Ferraz, M. Shakibaei, P. Martín-Vasallo, Glucose transport and metabolism in chondrocytes: a key to understanding chondrogenesis, skeletal development and cartilage degradation in osteoarthritis. *Histol. Histopathol.* **17**, 1239-1267 (2002).
58. C. L. Merrill, H. Ni, L. W. Yoon, M. A. Tirmenstein, P. Narayanan, G. R. Benavides, M. J. Easton, D. R. Creech, C. X. Hu, D. C. McFarland, L. M. Hahn, H. C. Thomas, K. T. Morgan, Etomoxir-induced oxidative stress in HepG2 cells detected by differential gene expression is confirmed biochemically. *Toxicol. Sci.* **68**, 93-101 (2002).
59. R. S. O'Connor, L. Guo, S. Ghassemi, N. W. Snyder, A. J. Worth, L. Weng, Y. Kam, B. Philipson, S. Trefely, S. Nunez-Cruz, I. A. Blair, C. H. June, M. C. Milone, The CPT1a inhibitor, etomoxir induces severe oxidative stress at commonly used concentrations. *Sci Rep* **8**, 6289 (2018).

60. M. M. Caron, P. J. Emans, M. M. Coolsen, L. Voss, D. A. Surtel, A. Cremers, L. W. van Rhijn, T. J. Welting, Redifferentiation of dedifferentiated human articular chondrocytes: comparison of 2D and 3D cultures. *Osteoarthr. Cartil.* **20**, 1170-1178 (2012).
61. A. Guermazi, D. Hayashi, F. W. Roemer, J. Niu, E. K. Quinn, M. D. Crema, M. C. Nevitt, J. Torner, C. E. Lewis, D. T. Felson, Brief Report: Partial- and Full-Thickness Focal Cartilage Defects Contribute Equally to Development of New Cartilage Damage in Knee Osteoarthritis: The Multicenter Osteoarthritis Study. *Arthritis & rheumatology (Hoboken, N.J.)* **69**, 560-564 (2017).
62. Y. Zhang, J. Mignone, W. R. MacLellan, Cardiac Regeneration and Stem Cells. *Physiol. Rev.* **95**, 1189-1204 (2015).
63. K. R. Jessen, R. Mirsky, P. Arthur-Farraj, The Role of Cell Plasticity in Tissue Repair: Adaptive Cellular Reprogramming. *Dev. Cell* **34**, 613-620 (2015).
64. J. Shan, R. E. Schwartz, N. T. Ross, D. J. Logan, D. Thomas, S. A. Duncan, T. E. North, W. Goessling, A. E. Carpenter, S. N. Bhatia, Identification of small molecules for human hepatocyte expansion and iPS differentiation. *Nat. Chem. Biol.* **9**, 514-520 (2013).
65. M. Oertel, A. Menthena, M. D. Dabeva, D. A. Shafritz, Cell competition leads to a high level of normal liver reconstitution by transplanted fetal liver stem/progenitor cells. *Gastroenterology* **130**, 507-520; quiz 590 (2006).
66. E. Moreno, Y. Fernandez-Marrero, P. Meyer, C. Rhiner, Brain regeneration in Drosophila involves comparison of neuronal fitness. *Curr. Biol.* **25**, 955-963 (2015).
67. M. K. Lotz, S. Otsuki, S. P. Grogan, R. Sah, R. Terkeltaub, D. D'Lima, Cartilage cell clusters. *Arthritis and rheumatism* **62**, 2206-2218 (2010).
68. F. Qu, F. Guilak, R. L. Mauck, Cell migration: implications for repair and regeneration in joint disease. *Nat Rev Rheumatol* **15**, 167-179 (2019).
69. P. Niemeyer, W. Köstler, G. M. Salzmann, P. Lenz, P. C. Kreuz, N. P. Südkamp, Autologous chondrocyte implantation for treatment of focal cartilage defects in patients age 40 years and older: A matched-pair analysis with 2-year follow-up. *Am J Sports Med* **38**, 2410-2416 (2010).
70. M. Gosset, F. Berenbaum, S. Thirion, C. Jacques, Primary culture and phenotyping of murine chondrocytes. *Nat Protoc* **3**, 1253-1260 (2008).
71. Y. Wen, Y. Chen, W. Wu, H. Zhang, Z. Peng, X. Yao, X. Zhang, W. Jiang, Y. Liao, Y. Xie, X. Shen, H. Sun, J. Hu, H. Liu, X. Chen, J. Chen, H. Ouyang, Hyperplastic Human Macromass Cartilage for Joint Regeneration. *Advanced science (Weinheim, Baden-Wurttemberg, Germany)* **10**, e2301833 (2023).
72. X. Han, R. Wang, Y. Zhou, L. Fei, H. Sun, S. Lai, A. Saadatpour, Z. Zhou, H. Chen, F. Ye, D. Huang, Y. Xu, W. Huang, M. Jiang, X. Jiang, J. Mao, Y. Chen, C. Lu, J. Xie, Q. Fang, Y. Wang, R. Yue, T. Li, H. Huang, S. H. Orkin, G. C. Yuan, M. Chen, G. Guo, Mapping the Mouse Cell Atlas by Microwell-Seq. *Cell* **172**, 1091-1107.e17 (2018).
73. H. Heaton, A. M. Talman, A. Knights, M. Imaz, D. J. Gaffney, R. Durbin, M. Hemberg, M. Lawniczak, Souporcell: robust clustering of single-cell RNA-seq data by genotype without reference genotypes. *Nat. Methods* **17**, 615-620 (2020).
74. F. A. Wolf, P. Angerer, F. J. Theis, SCANPY: large-scale single-cell gene expression data analysis. *Genome Biol.* **19**, 15 (2018).
75. S. Jin, C. F. Guerrero-Juarez, L. Zhang, I. Chang, R. Ramos, C. H. Kuan, P. Myung, M. V. Plikus, Q. Nie, Inference and analysis of cell-cell communication using CellChat. *Nat Commun* **12**, 1088 (2021).
76. T. Chen, X. Chen, S. Zhang, J. Zhu, B. Tang, A. Wang, L. Dong, Z. Zhang, C. Yu, Y. Sun, L. Chi, H. Chen, S. Zhai, Y. Sun, L. Lan, X. Zhang, J. Xiao, Y. Bao, Y. Wang, Z. Zhang, W. Zhao, The Genome Sequence Archive Family: Toward Explosive Data Growth and Diverse Data Types. *Genomics Proteomics Bioinformatics* **19**, 578-583 (2021).
77. Database Resources of the National Genomics Data Center, China National Center for Bioinformation in 2022. *Nucleic Acids Res.* **50**, D27-D38 (2022).
78. K. Xia, J. Zhu, J. Hua, Z. Gong, C. Yu, X. Zhou, J. Wang, X. Huang, W. Yu, L. Li, J. Gao, Q. Chen, F. Li, C. Liang, Intradiscal Injection of Induced Pluripotent Stem Cell-Derived Nucleus Pulposus-Like Cell-Seeded Polymeric Microspheres Promotes Rat Disc Regeneration. *Stem Cells Int* **2019**, 6806540 (2019).
79. Y. Hong, F. Zhou, Y. Hua, X. Zhang, C. Ni, D. Pan, Y. Zhang, D. Jiang, L. Yang, Q. Lin, Y. Zou, D. Yu, D. E. Arnot, X. Zou, L. Zhu, S. Zhang, H. Ouyang, A strongly adhesive hemostatic hydrogel for the repair of arterial and heart bleeds. *Nat Commun* **10**, 2060 (2019).
80. P. Mainil-Varlet, B. Van Damme, D. Nesic, G. Knutsen, R. Kandel, S. Roberts, A new histology scoring system for the assessment of the quality of human cartilage repair: ICRS II. *Am J Sports Med* **38**, 880-890 (2010).

Acknowledgements

The authors acknowledge William A. Horton from Oregon Health and Science University for generously providing the Col2-pd2EGFP transgenic mice. The authors also acknowledge Prof. Xiaohui Zou, Prof. Wei Wei, Dr. Chong Teng, Dr. Jiansong Chen, Dr. Weiliang Wu from Zhejiang University, for their help in the collection of human chondrocytes and cartilage tissues. The authors

thank Prof. Guogi Guo from Zhejiang University for his technical support in the cell capture procedure for single-cell RNA sequencing.

Funding: National Key Research and Development Program of China 2023YFB3813000 (HO). National Natural Science Foundation of China T2121004 (HO). National Natural Science Foundation of China 82394441 (HO). National Natural Science Foundation of China U23A6009 (YC).

Author contributions: Conceptualization: YC, JC, HO; Methodology: YC, YY, ZS, LL, JC, YL, YW, XL, WS, HW, YL, XZ, HO; Software: RT, KZ; Validation: YC, ZS, JL, HO; Formal analysis: YC, JC, JL, CA; Investigation: YC, YY, ZS, JC, YL, YW, JL, WS, XC; Resources: YL, WS, XC, WL, JG, HO; Data curation: RT; Visualization: YC, RT, JC, CA, DCH, HO; Supervision: YC, HO; Writing—original draft: YC, JC, DCH; Writing—review & editing: YC, JC, DCH, HO; Project administration: YC, HO; Funding acquisition: YC, HO.

Competing interests: A patent application (2024101287040) has been submitted to the China National Intellectual Property Administration (CNIPA). Authors declare that they have no competing interests.

Data and materials availability: All data are available in the main text or the supplementary materials. All data used to draw the conclusions in the study are present in the main article or the supplementary materials. The RNA sequencing data were deposited in the Genome Sequence Archive in National Genomics Data Center, China National Center for Bioinformation/Beijing Institute of Genomics, Chinese Academy of Sciences (https://ngdc.cncb.ac.cn/gsa-human, HRA006517)

Figures and captions

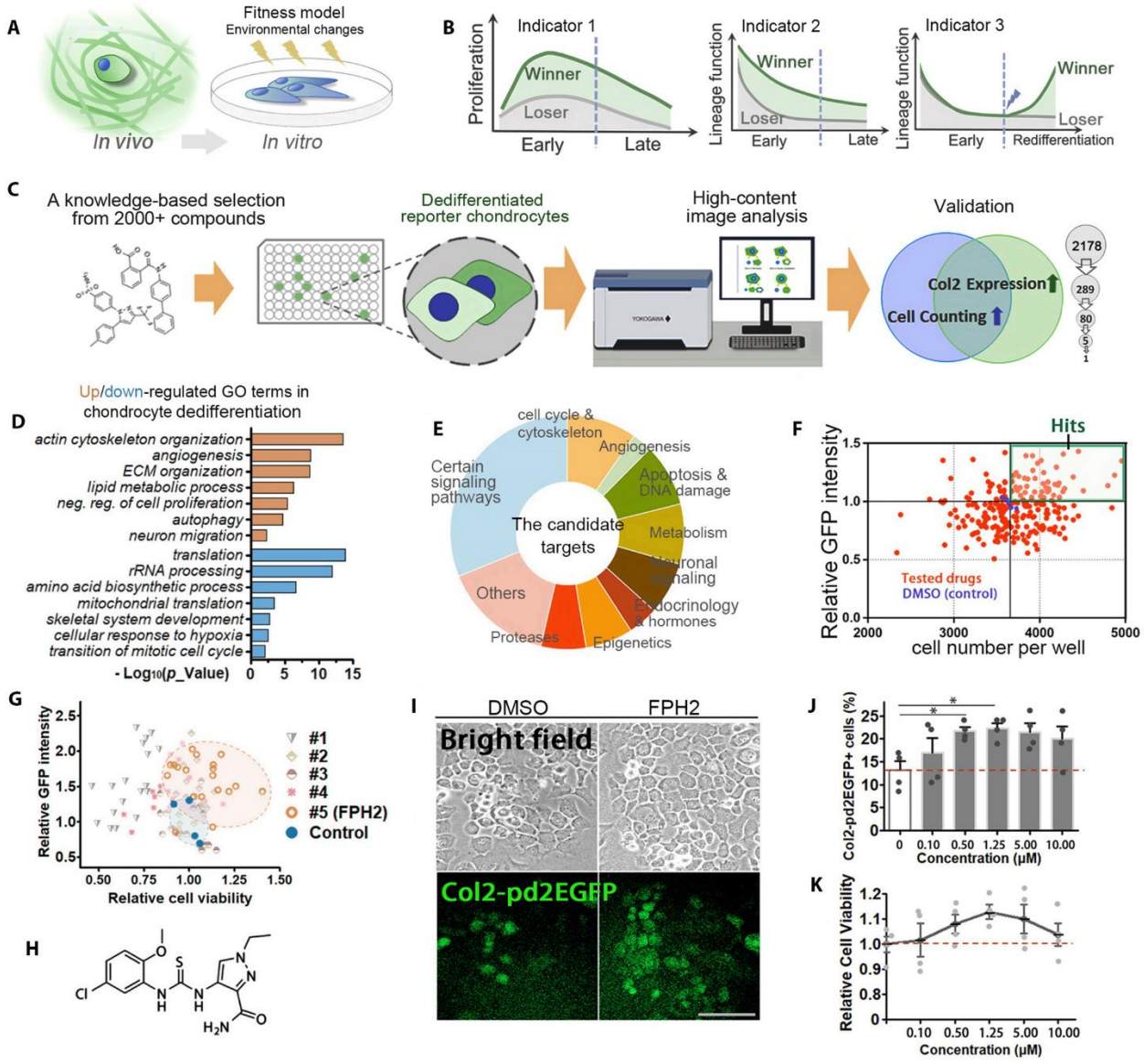

Fig.1 High-throughput screening to discover compounds driving chondrocyte cell fitness

(A) A schematic diagram shows that normoxia monolayer culture is a fitness model where chondrocytes grow against environmental changes after isolation from their in vivo niche.
(B) Expected performance of winner and loser cells in the detected models. Winner cells displayed faster growth and delayed functional loss, as well as a rapid phenotype recovery after redifferentiation.
(C) The workflow of the high-throughput phenotypic-based drug screen with Col2-pd2EGFP reporter chondrocytes.
(D) Representative gene ontology (GO) terms of up- and down-regulated genes in dysfunctional/dedifferentiated chondrocytes compared to primary chondrocytes according to our previous data (GSE193742), providing potential targets for manipulating chondrocyte fitness.
(E) The class of candidate drug targets, inspired by the dedifferentiation-relevant GO terms.
(F) Potential hits (at a concentration of 1μM) that increased cell proliferation and the expression of

chondrocyte phenotype marker collagen type II (COL2) after a 48-hour treatment. Cells treated by dimethyl sulfoxide (DMSO group) served as the control (blue dots around the zero point).
(G) FPH2 exhibited an evident effect on both cell viability and chondrocyte functional phenotype when compared to other candidates. DMSO group served as the control (blue dots).
(H) The chemical structure of FPH2.
(I)~(K) Representative images and quantitative analysis of functional phenotype and cell number after a 48-hour FPH2 treatment on Col2-pd2EGFP reporter chondrocytes (passage 2, P2); scale bar: 100 μm.
All data are the mean ± SEM. *p <0.05, **p < 0.01, ***p <0.001.

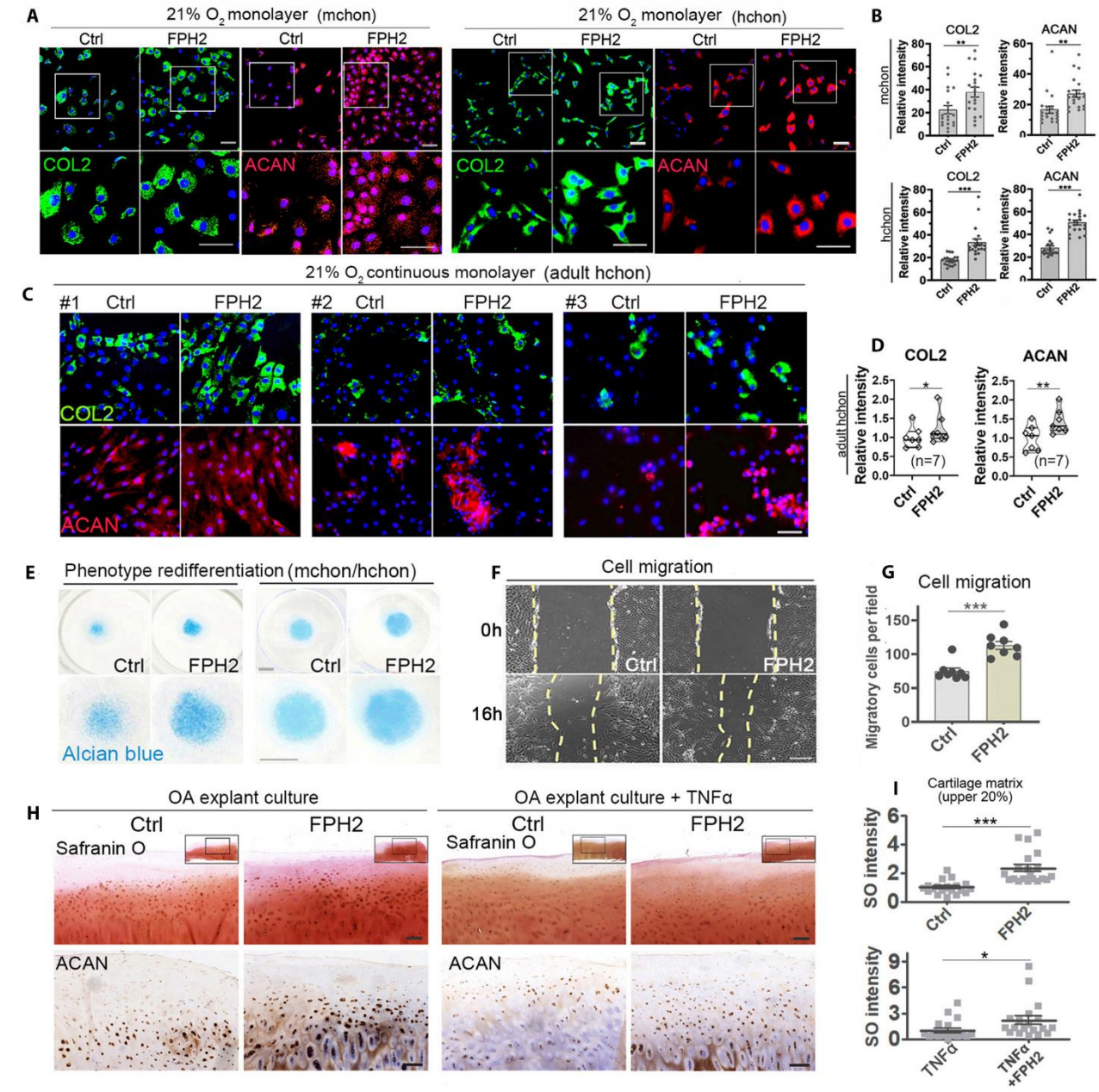

Fig.2 FPH2 improved chondrocyte performance in multiple tasks in vitro

(A)~(B) FPH2 benefited the phenotype maintenance of both mouse (mchon, P4) and human chondrocytes (hchon, P4) in a normoxia (21% O_2) monolayer culture. Representative images and quantitative analysis of immuno-stained cartilage lineage markers collagen type II (COL2) and aggrecan (ACAN); scale bar: 60 μm.

(C)~(D) FPH2 benefited the phenotype maintenance of adult human chondrocytes (n = 7) in continuous monolayer culture (P1~4). Representative images of 3 donors' samples were shown (another 4 were in fig. S1D); scale bar: 100 μm.

(E) FPH2 benefited the phenotype recovery of mouse (P4 mchon, left) and human chondrocytes (P4 hchon, right) in a micromass redifferentiation model; scale bar: 3mm.

(F)~(G) FPH2 promoted the migration behavior of human chondrocytes. Representative images and quantitative analysis of wound healing assay; scale bars: 200 μm.
(H)~(I) FPH2 benefited the cartilage phenotype maintenance against inflammation in an explant model. (H) Representative images of safranin O (SO) staining and immunochemistry staining of ACAN in human cartilage explants derived from osteoarthritis patients, cultured in serum-free medium with or without inflammatory factor tumor necrosis factor (TNF)-α; scale bar: 200 μm. (I) Quantitative analysis of safranin O staining intensity in the upper part (20%) of cartilage explants (joint surfaces).
All FPH2-treated samples were treated by 1μM FPH2 and the control groups were treated by 0.002% DMSO. Cells were treated for 48 hours and explants were cultured with FPH2 for 3 weeks. All data are the mean ± SEM. *p <0.05, **p < 0.01, ***p <0.001.

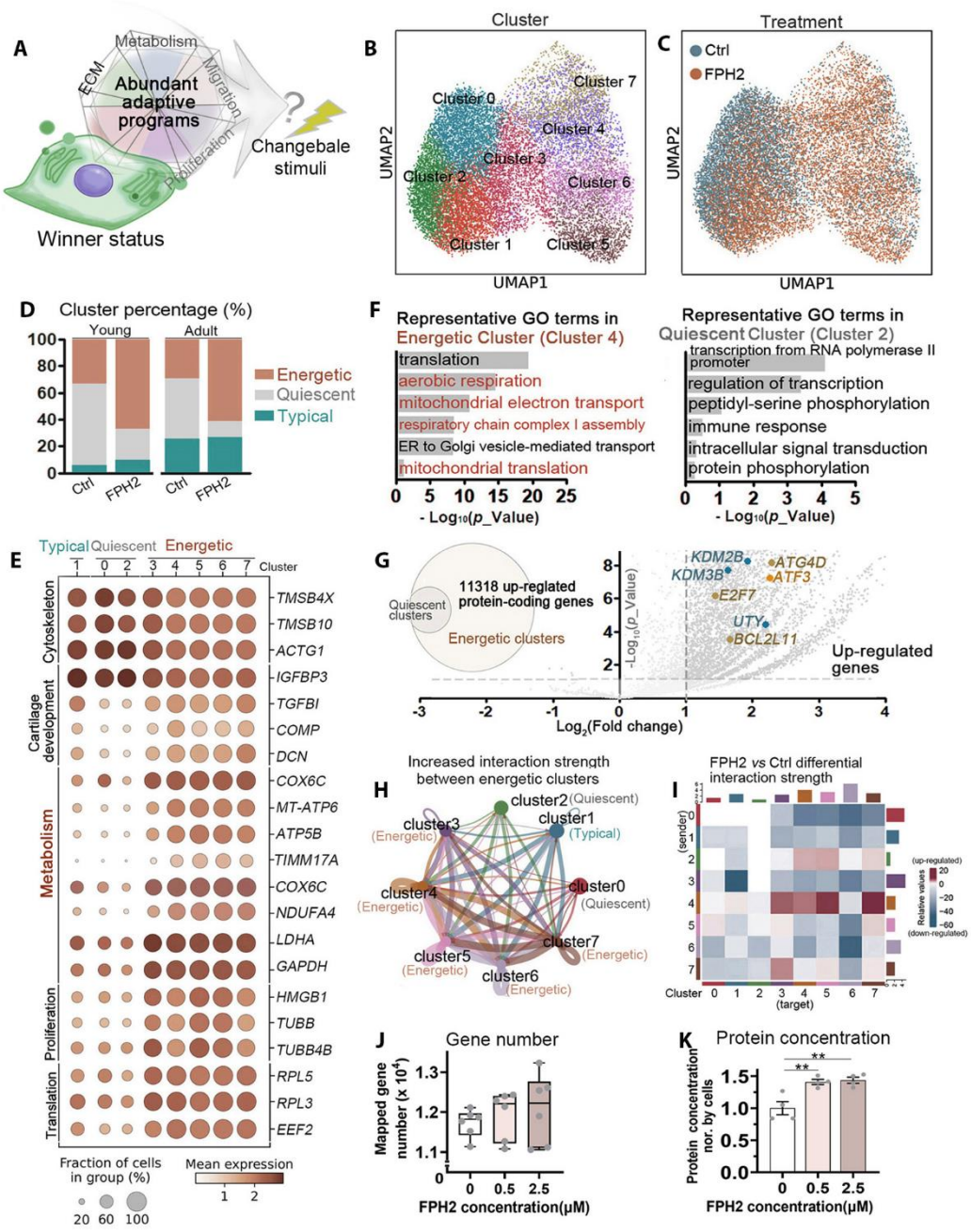

Fig. 3 FPH2-programmed winner cells expressed high levels of fitness-associated genes

(A) A summary diagram showing that FPH2 induced a cell status expressing abundant fitness/adaptation regulatory genes (cell phenotype, proliferation, migration and metabolism etc.), which potentially provided a "saturated rescue" program to maintain cell homeostasis in changeable environments

(B)~(C) Uniform manifold approximation and projection (UMAP) plots showing that FPH2-treated human chondrocytes and the controls were classified into 8 clusters based on the single-cell RNA sequencing analysis.

(D) FPH2 significantly increased the proportion of energetic clusters in both young (n = 4) and adult (n = 4) chondrocytes.

(E) Representative genes in the 8 clusters. Energetic: Cluster 3-7; Quiescent: Cluster 0 and 2; Typical chon (the typical chondrocytes): Cluster 1.
(F) Enriched gene ontology (GO) terms in the representative energetic cluster (Cluster 4) and quiescent cluster (Cluster 2) respectively.
(G) Venn and volcano plots showing that energetic clusters highly expressed protein-encoding genes relative to quiescent clusters.
(H) A circle plot showing that the interaction strength was higher between energetic clusters (Cluster 3-7) relative to that between other clusters. The edge width is proportional to the interaction probability or score.
(I) A heatmap showing the interaction strength between the 8 clusters (senders to targets). Red represents FPH2-induced up-regulation and blue stands for the down-regulation of interaction strength.
(J) FPH2 slightly increased the gene number expressed in murine chondrocytes, detected by bulk RNA sequencing (sample = 6).
(K) FPH2 significantly increased the total protein concentration in human chondrocytes (sample = 4). The protein concentration value was normalized by cell numbers.
All FPH2-samples were treated by 1μM FPH2 for 48 hours prior to cell capture and sequencing. All data are the mean ± SEM. *p <0.05, **p < 0.01, ***p <0.001.

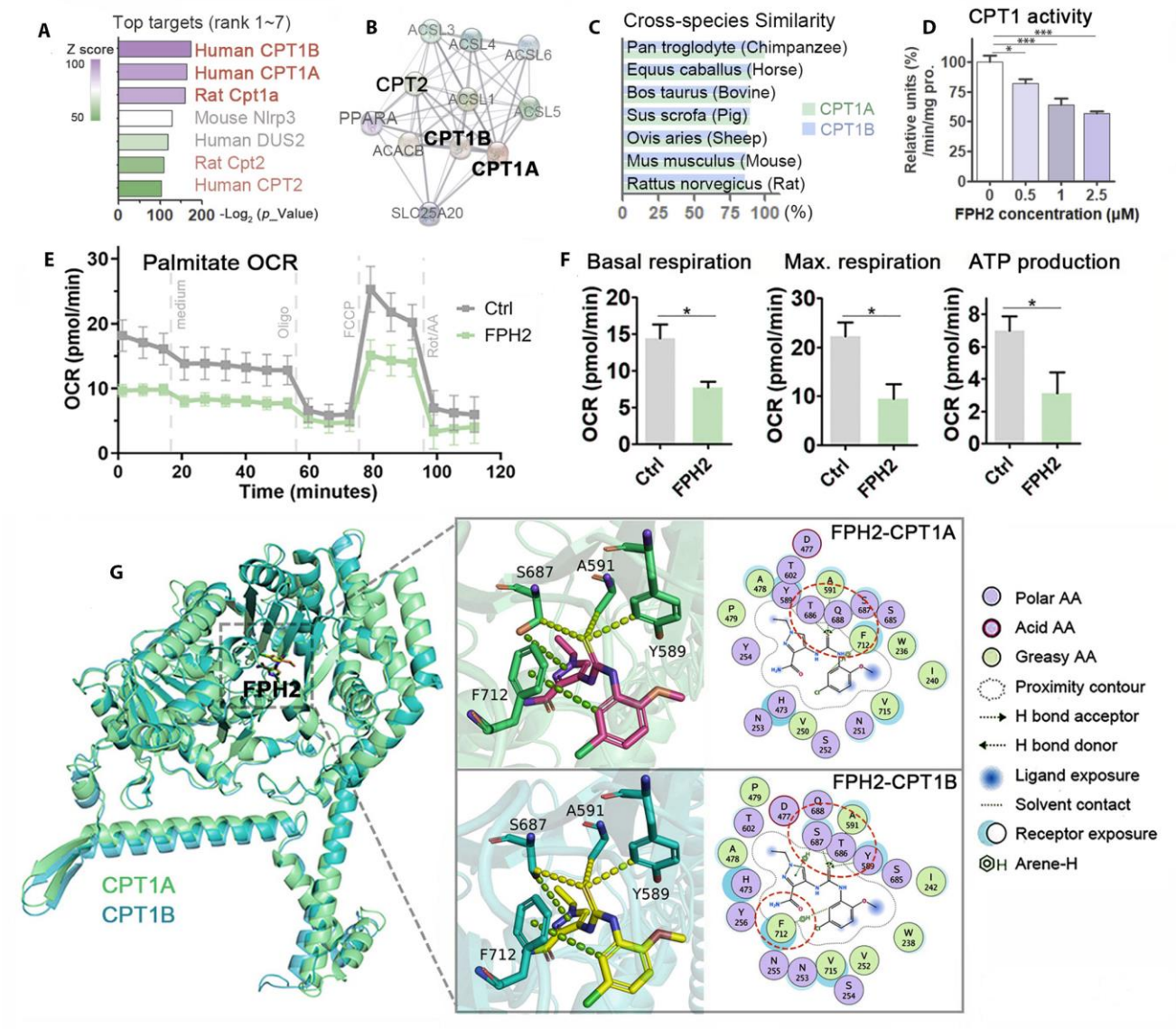

Fig. 4 FPH2 inhibited the activity of carnitine palmitoyl transferase I

(A) The candidates of FPH2's target in Similarity Ensemble Approach prediction.
(B) A STRING protein network shows that CPT1A/B play a key role in lipid metabolism.
(C) The similarity of CPT1A/B amino acid sequences in different species, indicating that CPT1 is a highly conserved protein.
(D) FPH2 significantly inhibited the activity of carnitine palmitoyl transferase I (CPT1), detected by a CPT1 activity assay kit.
(E)~(F) Palmitate oxygen consumption rate (OCR) assays illustrate that FPH2 significantly suppressed fatty acid oxidation (FAO) when palmitate was offered as the substrate for energy production. Particularly, FPH2 treatment evidently reduced the basal respiration, maximal respiration and ATP production level of palmitate-OCR. The FPH2 group was pre-treated by 1μM FPH2 for 48 hours prior to the test (n = 5), and the control was treated by 0.002% DMSO (n = 6).
(G) Molecular docking analysis showes the inferred binding mode of FPH2 with human CPT1A/B. (Left)

A three-dimensional (3D) view showing the best-ranked pose of binding (CPT1A: green; CPT1B: cyan blue). (Right) 3D images and two-dimensional (2D) cartoons showing FPH2's interaction with surrounding amino acids (Y589, A591, S687 and F712). (Upper) 3D structure of FPH2: carbon atoms in magenta; oxygen atoms in red; nitrogen atoms in blue; chlorine atoms in green. (Lower) 3D structure of FPH2: carbon atoms in yellow; oxygen atoms in red; nitrogen atoms in blue; chlorine atoms in green. In 3D views, the yellow dashed line represents the hydrogen bonding interaction, while the green dashed line represents the arene-hydrogen interaction. In 2D views, the green arrow represents hydrogen bonding, and the green dashed line represents the arene-hydrogen interaction.
All data are the mean ± SEM. *p <0.05, **p < 0.01, ***p <0.001.

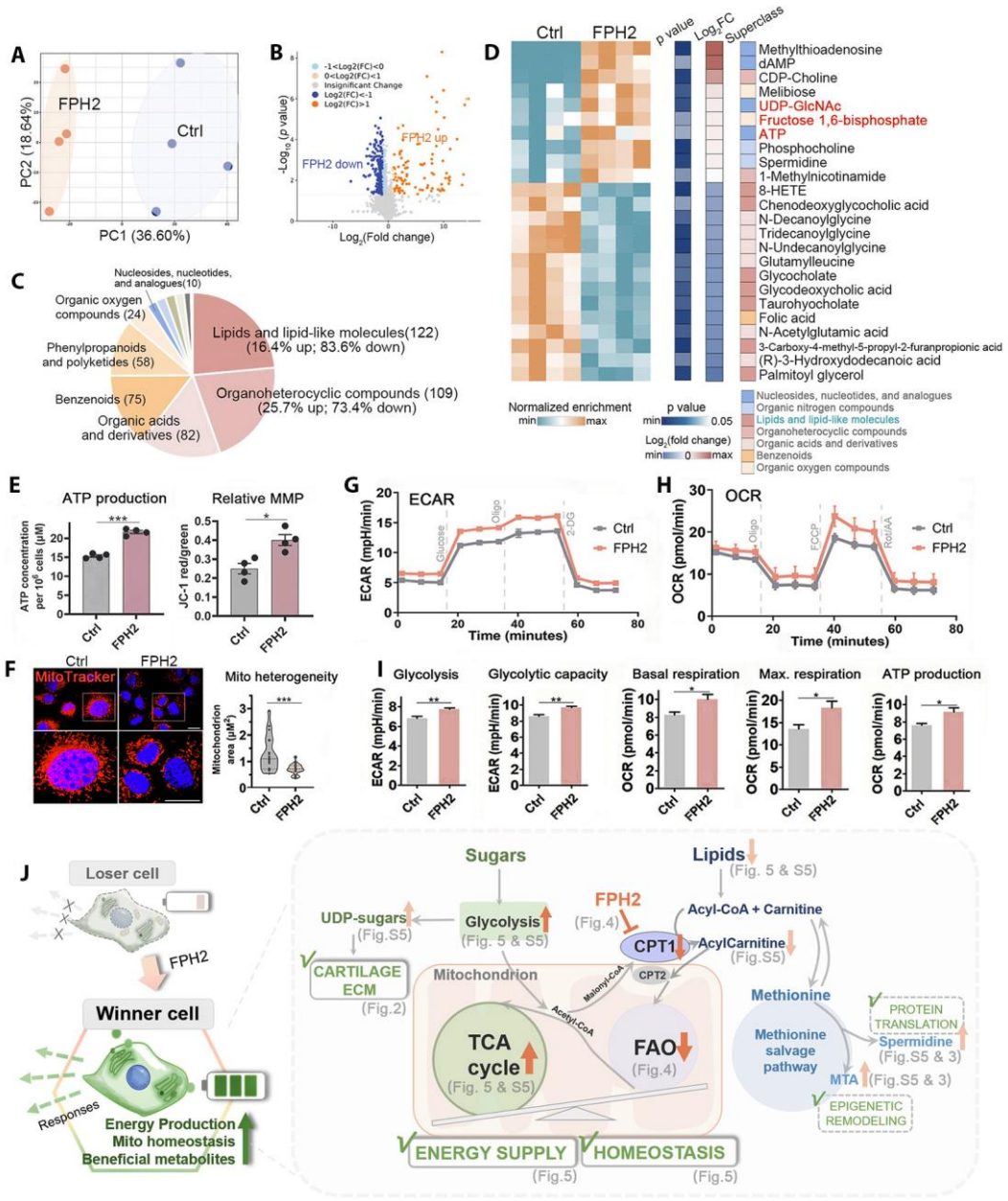

Fig. 5 FPH2 induced an optimal metabolic pattern and boosted energy production

(A) A principal component analysis (PCA) plot shows the distinct metabolic profiling in FPH2-treated cells and the controls (n = 4). The FPH2 group was treated by 2.5 μM FPH2 for 48 hours and the control group was treated by equal amount of DMSO.

(B) A volcano plot shows the significantly differentially regulated metabolites in FPH2 group relative to the controls.

(C) A pie chart shows that lipids and lipids molecules belonged to the most abundant class in the significantly differentially regulated metabolites.

(D) A heatmap displays representative differentially regulated metabolites in FPH2 group relative to the controls.

(E) FPH2 enhanced ATP production and mitochondrial membrane potential (MMP) in murine chondrocytes. The FPH2 group was treated by 1μM FPH2 for 48 hours prior to the test.

(F) Representative images and quantitative analysis showing that FPH2 reduced the heterogeneity in mitochondrial morphology of murine chondrocytes; scale bars: 20 μm. The FPH2 group was treated by 1μM FPH2 for 48 hours prior to the examination.
(G)~(I) Extracellular acidification rate (ECAR) and OCR analysis showing that FPH2 significantly improved glycolysis level and the ATP production in the mitochondrial respiration of chondrocytes. The FPH2 group was pre-treated by 1μM FPH2 for 48 hours prior to the test ($n > 10$ for each group).
(J) A schematic diagram illustrates that FPH2-treated chondrocytes obtained an energetic winner phenotype with a higher level of energy production, a more stable mitochondrial homeostasis, and an improved accumulation of beneficial metabolites. Potential mechanisms were concluded from our metabolomics and other live-cell tests, including the inhibition of CPT1 and FAO, as well as the alterations in sugar and amino acid metabolism.
All data are the mean ± SEM. $*p < 0.05$, $**p < 0.01$, $***p < 0.001$.

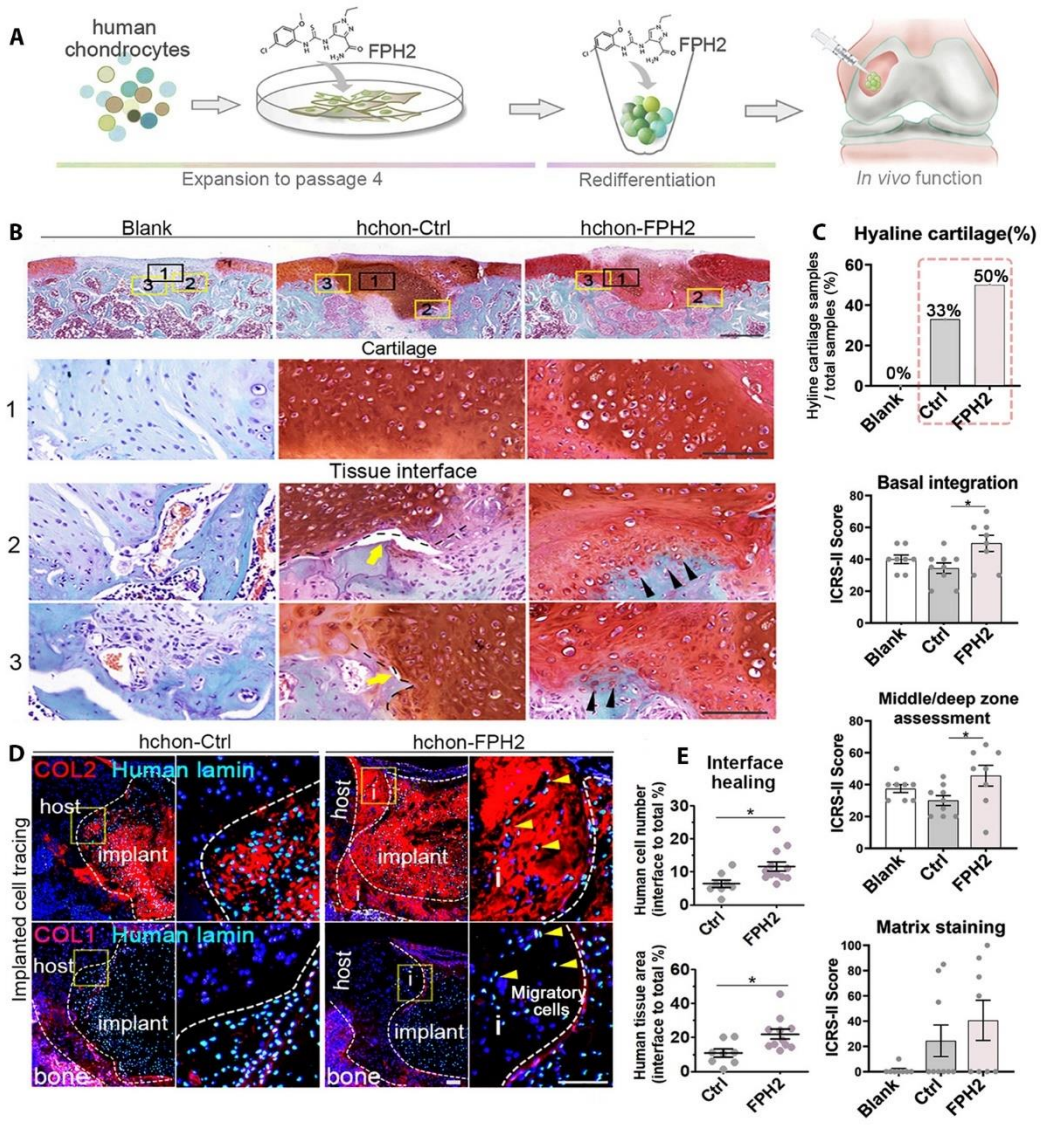

Fig. 6 FPH2 improved cell fitness and cartilage regeneration in vivo

(A) A strategic diagram shows a workflow simulating the pre-implantation cell culture in autologous chondrocyte implantation (ACI), which adopted FPH2 (1μM) in the continuous expansion (monolayer culture till P4, followed by a redifferentiation induction) of human adult chondrocytes (n=6). Cells isolated from same donors and were treated with 0.002% DMSO during the whole culture process as controls (hchon-Ctrl). Then the pellets were then implanted in a full-thickness cartilage defect model in rats.

(B) FPH2-treated chondrocytes formed hyalin cartilage in vivo with an improved tissue integration. Representative images of safranin O-stained joint tissues collected 12 weeks post surgery. Blank group: defects without implants; hchon-FPH2 and hchon-Ctrl group: defects with FPH2-treated implants and DMSO-cultured implants, respectively; yellow arrows: gaps between the hosts and implants; black arrows: cells growing in the interfaces; scale bar: 500 μm (Row1); 100 μm (Row 2-4, zoom-in images).

(C) Quantitative analysis and ICRS-II scoring demonstrating a higher potential of hyaline cartilage formation and a higher level of implant-host tissue integration (basal integration) in FPH2 group.

(D) FPH2-treated chondrocytes showed an enhanced migratory phenotype in vivo, which could promote tissue interfaces healing. Representative images showing the immuno-stained colocalization of cartilage

marker COL2 and fibrosis/bone marker COL1 with human nuclear marker Lamin A/C; i: the region of implant-host interfaces; yellow arrows: human cells that grew into the surrounding tissues; scale bar: 100 μm;
(E) Quantitative analysis shows that FPH2-induced human chondrocytes made an elevated contribution to the healing of tissue interfaces (cell number and tissue area).
All data are the mean ± SEM. *p <0.05, **p < 0.01, ***p <0.001.

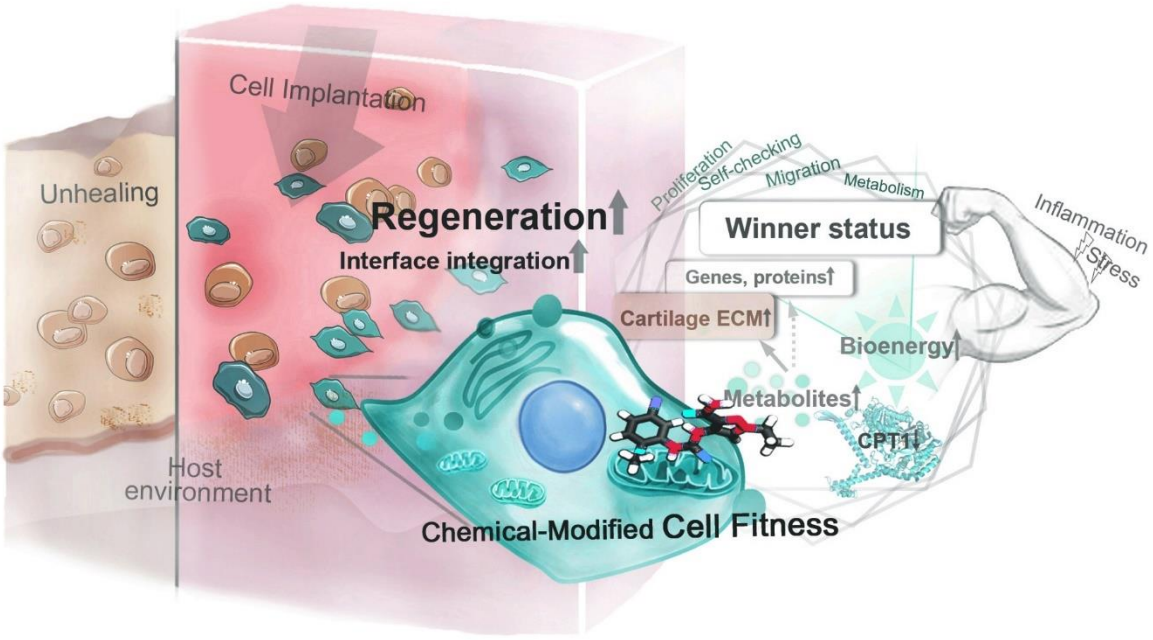

Fig. 7 FPH2 effectively empowers cell fitness for cartilage regeneration

This study illustrates an advantageous chemical approach for cell fitness manipulation in tissue regeneration. The small molecular compound FPH2 induces a winner cell status highly expressing multiple fitness-responsible programs and obtaining a chondrocyte-beneficial metabolism.

This Supplementary Materials file includes:

Figure S1 to S11

Table S1 to S2

Other Supplementary Materials for this manuscript include the following:

Data S1 to S3

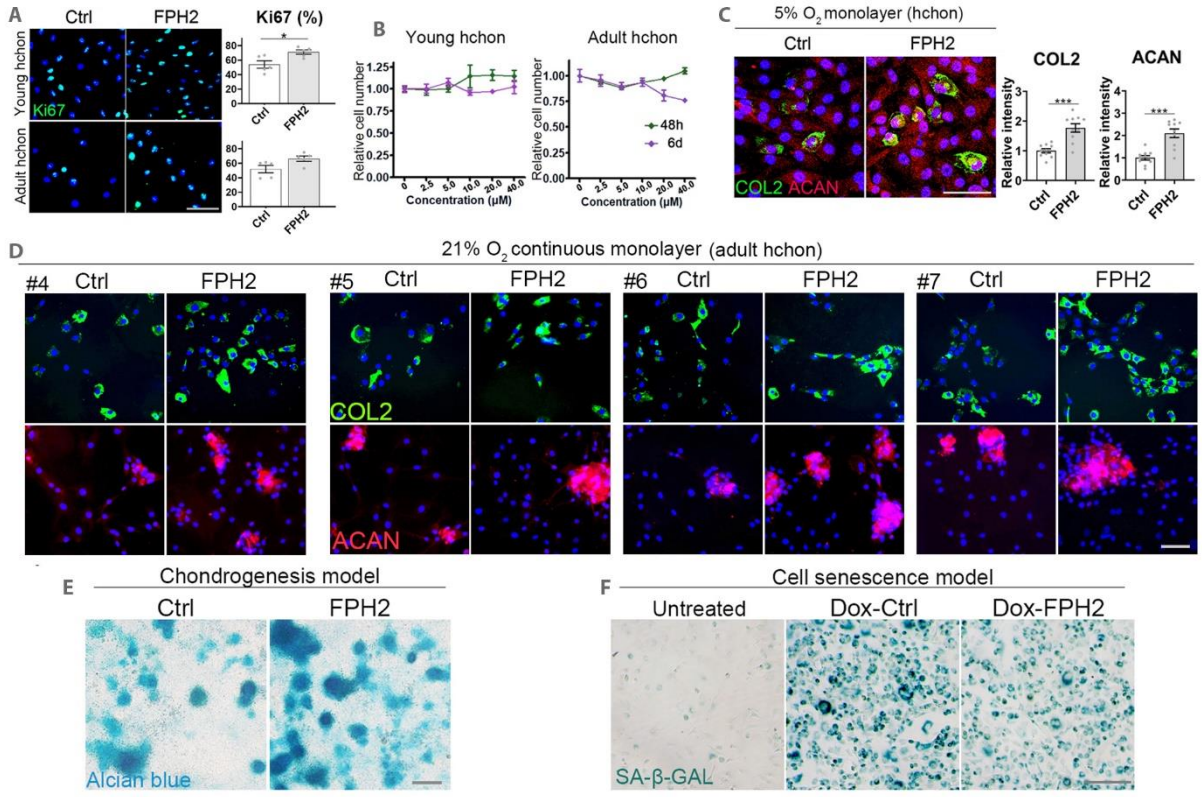

Fig. S1. FPH2 improved chondrocyte performance in multiple tasks in vitro.

(**A**) Representative images and quantitative analysis of immune-stained proliferative marker Ki67 in human young and adult chondrocytes; scale bar: 100 μm. 1μM FPH2 was applied to a 48-hour culture.

(**B**) Short-term and long-term cytotoxicity of FPH2 in human young and adult chondrocytes.

(**C**) FPH2 treatment benefited the phenotype maintenance of human chondrocytes in hypoxia (5% O_2) monolayer culture; scale bar: 50 μm. FPH2- samples were treated by 1μM FPH2 for 48 hours and the control group was treated by 0.002% dimethyl sulfoxide (DMSO).

(**D**) FPH2 treatment benefited the phenotype maintenance of adult human chondrocytes (n = 7) in continuous monolayer culture (passage 1~4). Representative images of 4 donors' samples were shown (the others were in Fig. 1C); scale bar: 100 μm. FPH2- samples were treated by 1μM FPH2 for 48 hours and the control group was treated by 0.002% DMSO.

(**E**) FPH2 treatment increased the chondrogenic phenotype in an ATDC5 chondrogenesis model; scale bars: 500 μm. 1μM FPH2 was applied to ATDC5 chondrogenesis induction for 7 days.

(**F**) FPH2 treatment slightly decreased the age-related phenotype in a doxorubicin (Dox)-induced senescence model; scale bars: 100 μm. Murine chondrocytes were induced with 100nM Dox for 24 hours and then treated with 2.5 μM FPH2 for 7 days. The senescence-like phenotype was identified by β-Galactosidase staining.

All data are the mean ± SEM. **p* <0.05, ***p* < 0.01, ****p* <0.001.

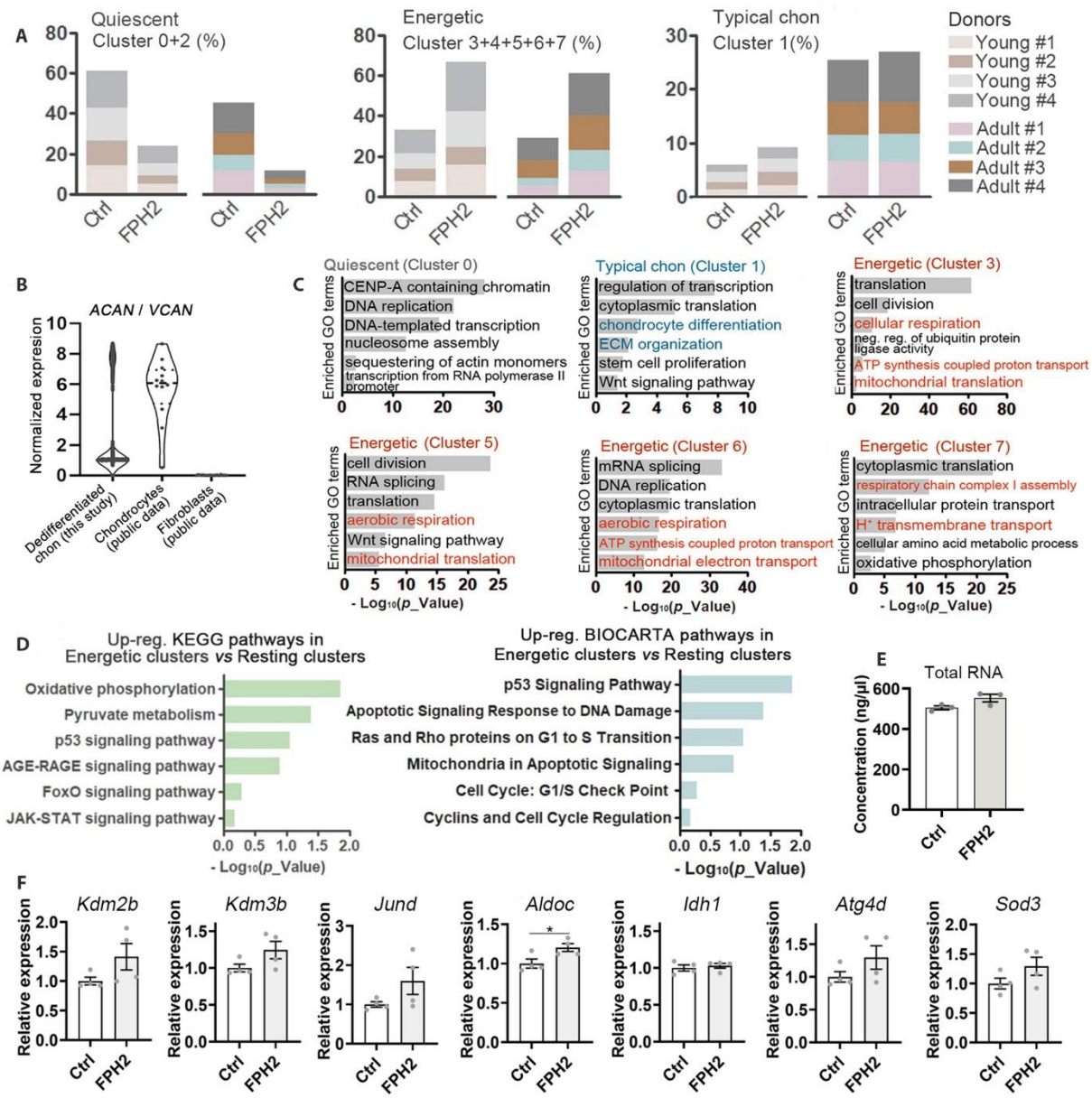

Fig. S2. FPH2 endowed chondrocytes with a winner status.

(**A**) The proportion changes of quiescent, energetic and typical chondrocyte clusters in treated and untreated samples (4 young and 4 adult donors' chondrocytes).

(**B**) Comparison of the expression pattern of cell identity markers (ratio of *ACAN* (aggrecan) / *VCAN* (versican)) in detected dedifferentiated chondrocytes in single-cell analysis, normal chondrocytes (positive controls from public datasets) and synovial fibroblasts (negative controls from public datasets), suggesting that the detected cells preserved their chondrocyte identity and were still distinctive from fibroblasts. Public data were collected from MSdb database (https://www.msdb.org.cn/). The data used in the analysis are GSE106292 (sample ID GSM2871645, GSM2871646, GSM2871647), GSE114007 (sample ID GSM3130549 ~ GSM3130558) and GSE176223 (sample ID GSM5360334 ~ GSM5360356).

(**C**) Representative enriched gene ontology (GO) terms in the quiescent cluster (Cluster 0) typical chondrocyte cluster (Cluster 1) and energetic clusters (Cluster 3, 5, 6 and 7).
(**D**) Representative up-regulated KEGG and BIOCARTA pathways in energetic clusters compared to quiescent clusters, indicating an activation of metabolic and fitness regulatory programs.
(**E**) FPH2-treated chondrocytes displayed a slight increase of RNA concentration after RNA isolation from the same amount of cells (sample =3).
(**F**) FPH2 treatment broadly upregulated fitness-associated genes in chondrocytes (sample = 4), detected by real-time qPCR.
For RNA isolation and qPCR, murine chondrocytes were treated by 1 μM FPH2 for 48 hours prior to the test. DMSO was added as the control.
All data are the mean ± SEM. **p* <0.05, ***p* < 0.01, ****p* <0.001.

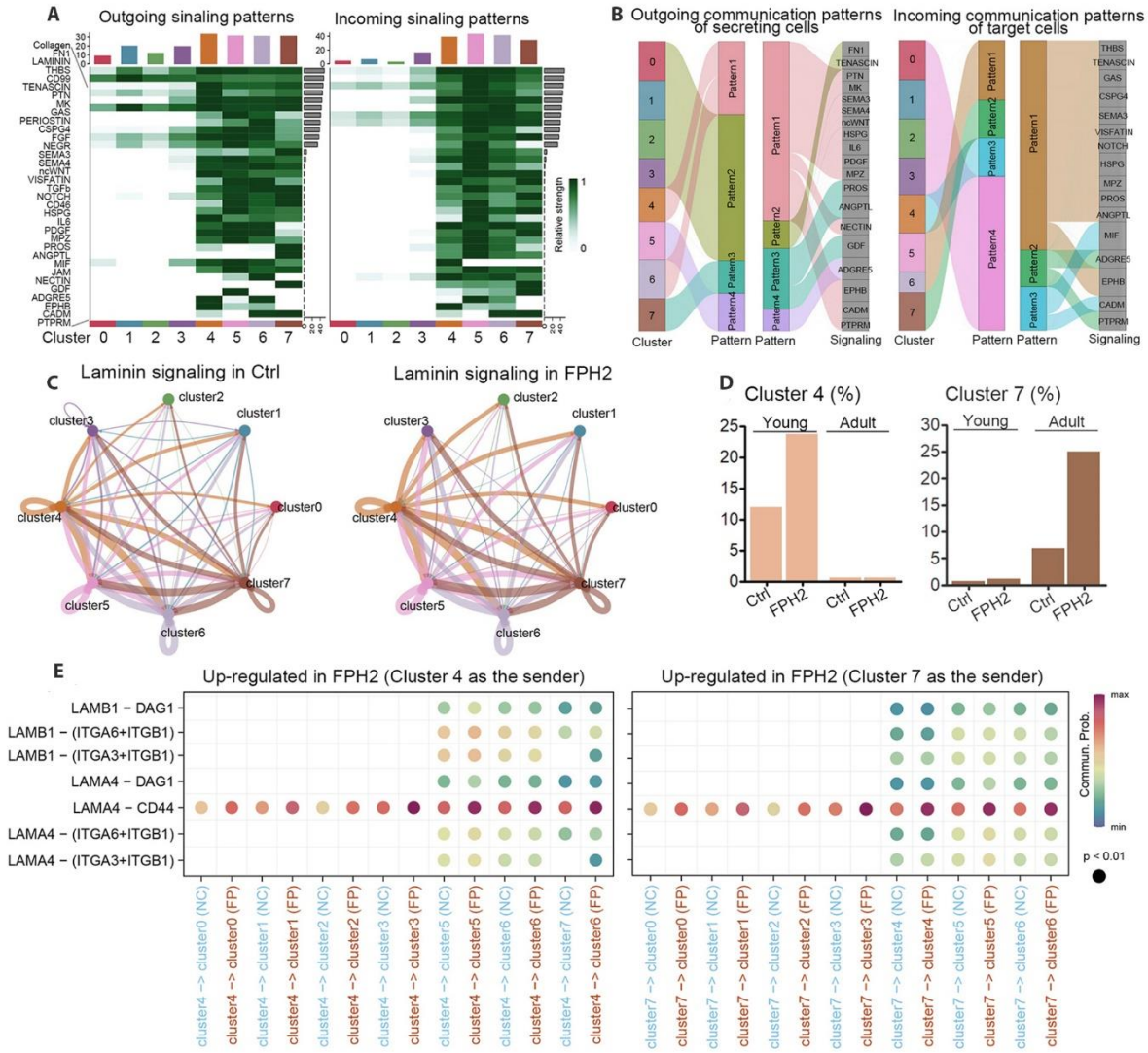

Fig. S3. Energetic and quiescent clusters exhibited distinct patterns of intercellular communication.

(**A**) Estimated strength of representative outgoing and incoming signaling patterns in the 8 clusters.
(**B**) Inferred outgoing and incoming communication patterns in the 8 clusters, representing the links between the cell clusters, patterns and pathways. The flow thickness indicates the contribution of the clusters or pathways to each pattern.
(**C**) Intercellular communication network of Laminin signaling was inferred to be up-regulated in FPH2 groups, especially for the interaction pairs that Cluster 4 and 7.
(**D**) The proportion of the most prevalent energetic clusters in young and adult cells (Cluster 4 and 7) were significantly increased after FPH2 treatment.
(**E**) Communication probability of specific ligand-receptor pairs in Laminin signaling pathways sent by Cluster 4 and 7 respectively, indicating that FPH2 positively regulated the outgoing communication of Laminin pathways in energetic cells.

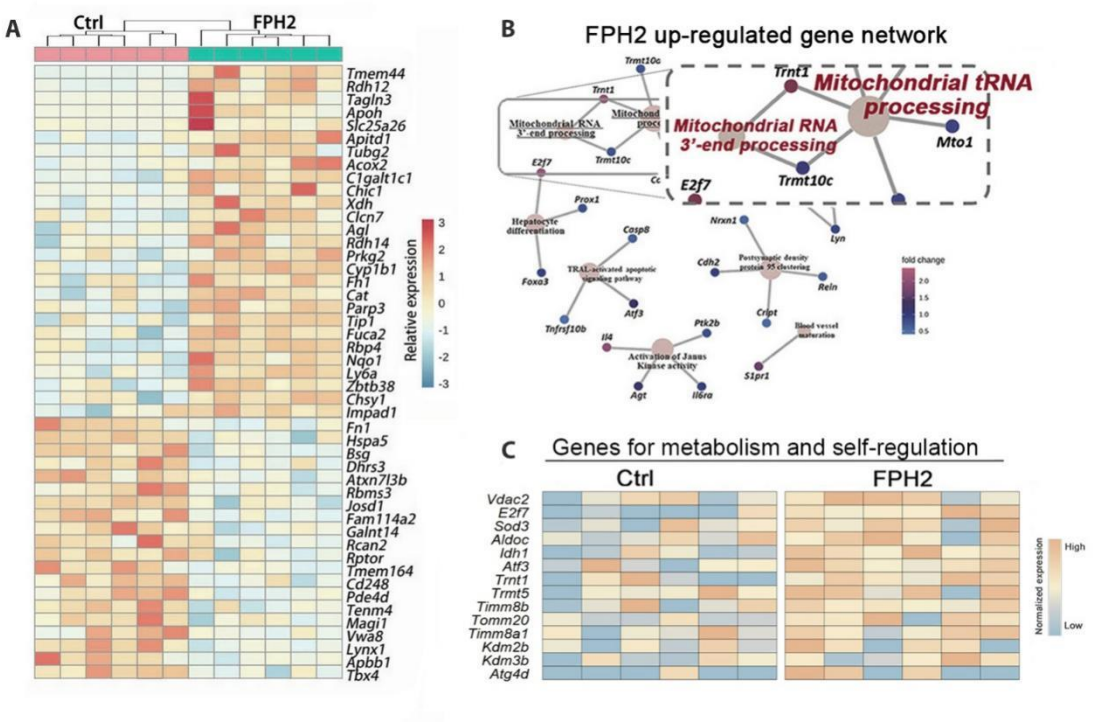

Fig. S4. Bulk-RNA sequencing revealed that FPH2 up-regulated metabolic-associated programs.

(**A**) Representative differentially expressed genes in FPH2-treated murine chondrocytes relative to the controls.

(**B**) Up-regulated gene network showing an activation of genes relevant to mitochondrial RNA processing in FPH2 group.

(**C**) Representative genes regulating metabolism and cell self-regulation that were up-regulated by FPH2.

Murine chondrocytes were treated by 2.5 μM FPH2 for 48 hours and the control group was treated by the same amount of DMSO prior to the RNA sequencing.

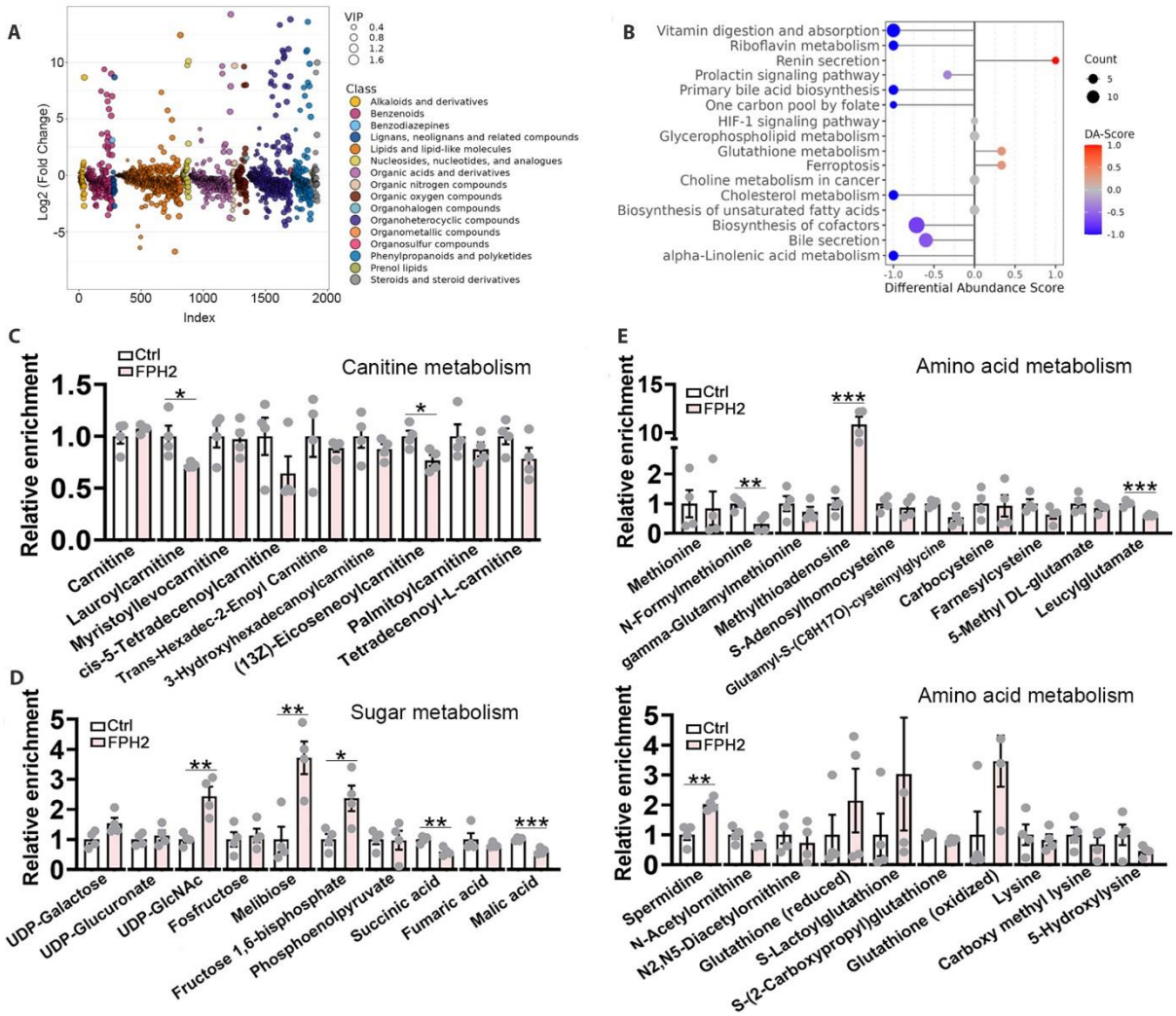

Fig. S5. FPH2 induced alterations in metabolic pattern and metabolite accumulation.

(**A**) The class of regulated metabolites in FPH2 group relative to the controls. The plot was resulted from orthogonal partial least-square discriminant analysis (OPLS-DA) of metabolic profiling data; VIP: the variable importance on projection.

(**B**) Representative differentially enriched KEGG pathways in FPH2 group relative to the controls; DA-score: differential abundance score.

(**C**)~(**E**) Representative FPH2-induced metabolite abundance changes in carnitine, sugar and amino acid metabolism.

The FPH2 group was treated by 2.5 μM FPH2 for 48 hours and the control group was treated by 0.005% DMSO.

All data are the mean ± SEM. **p* <0.05, ***p* < 0.01, ****p* <0.001.

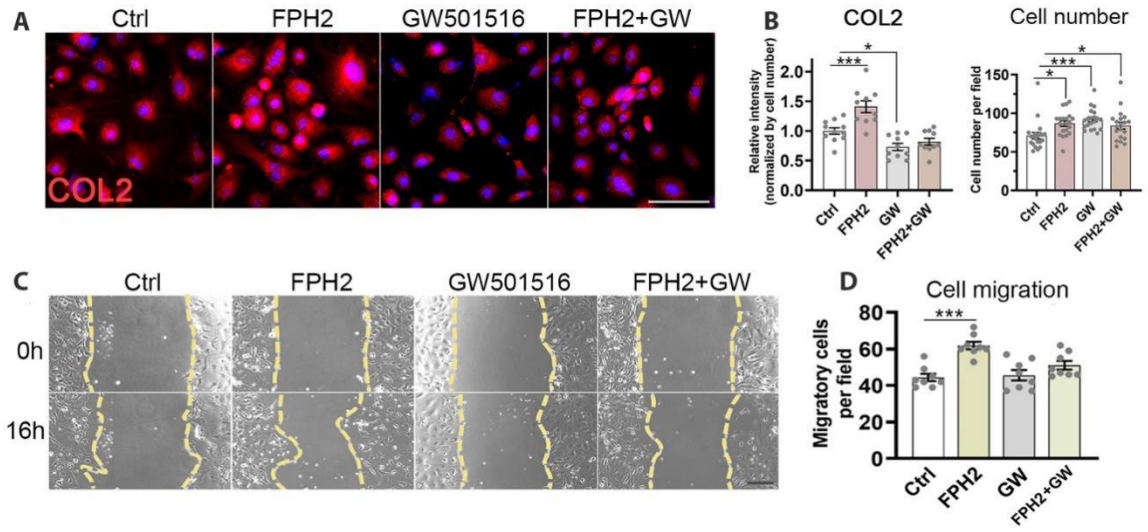

Fig. S6. Activation of fatty acid oxidation reduced chondrocyte functional phenotype.

(**A**) Representative images and quantitative analysis of immune-stained collagen type II (COL2) in chondrocytes treated by FPH2 and GW501516 (a PPAR agonist, shown to activate fatty acid oxidation), suggesting that activation of fatty acid oxidation induced a negative effect on chondrocyte phenotype maintenance; scale bars: 100 μm. Samples were treated by 1 μM FPH2 or 1μM GW501516 or both for 48 hours prior to the test. DMSO was equally added in each group.
(**B**) Quantitative analysis of COL2 expression and cell number, indicating that GW50156 slightly promoted cell proliferation but did not improve chondrocyte phenotype maintenance.
(**C**)~(**D**) Representative images and quantitative analysis of wound healing assay, demonstrating that GW501516 did not effectively promote chondrocyte migration as FPH2; scale bars: 200 μm. Samples treated by 1 μM FPH2 or 1μM GW501516 or both for 16 hours (overnight) in serum-free medium prior to the test. DMSO was equally added in each group.
All data are the mean ± SEM. **p* <0.05, ***p* < 0.01, ****p* <0.001.

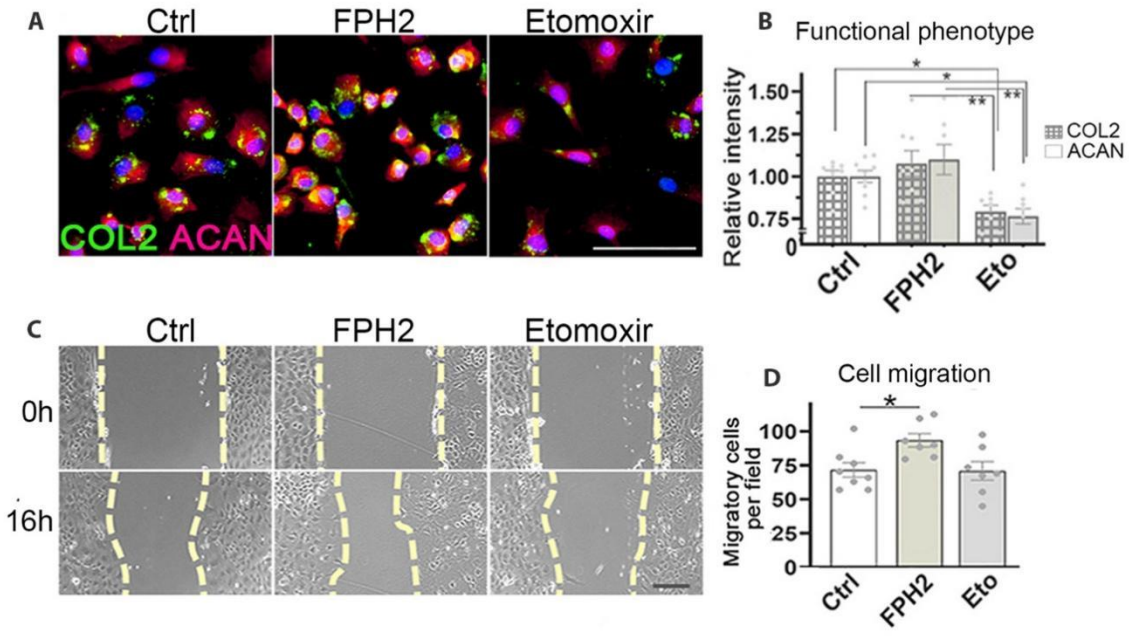

Fig. S7. The irreversible inhibitor Etomoxir did not induce similar effects as FPH2.

(**A**)~(**B**) Representative images and quantitative analysis of immune-stained COL2 and ACAN in chondrocytes treated by FPH2 and Etomoxir (Eto), suggesting that Eto did not significantly benefit chondrocyte culture and phenotype maintenance as FPH2; scale bars: 100 μm. Samples were treated by 1 μM FPH2 or 2μM Eto for 48 hours prior to the test. DMSO was equally added in each group.

(**C**)~(**D**) Eto did not effectively promote chondrocyte migration as FPH2; scale bars: 200 μm. Samples treated by 1 μM FPH2 or 2μM Eto for 16 hours (overnight) in serum-free medium prior to the test. DMSO was equally added in each group.

All data are the mean ± SEM. **p* <0.05, ***p* < 0.01, ****p* <0.001.

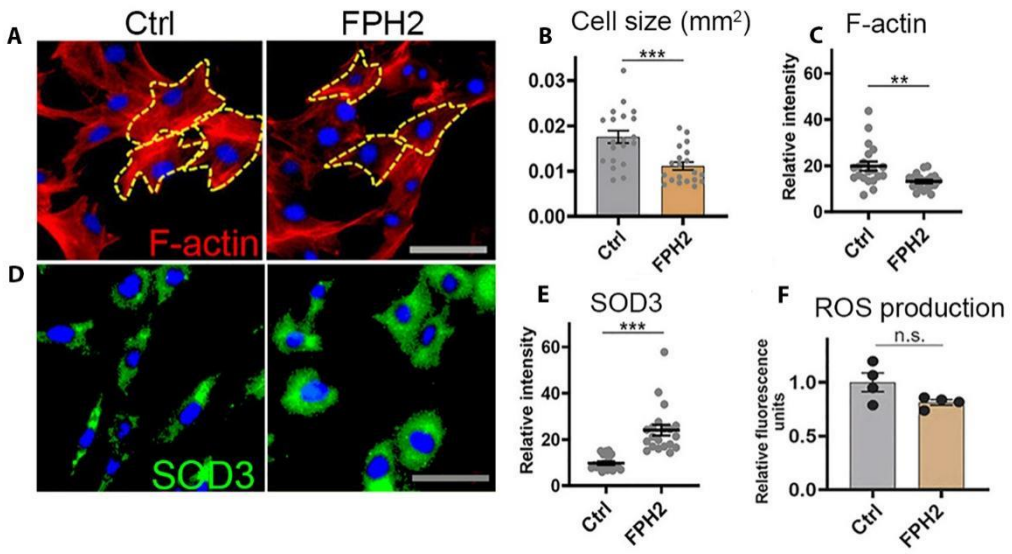

Fig. S8. FPH2 decreased cell size and facilitated mitochondrial homeostasis.

(**A**)~(**C**) FPH2-treated chondrocytes showed a reduced cell size and a reduced expression of actin fibers; scale bars: 50 μm.

(**D**)~(**E**) FPH2-treated chondrocytes showed an increased expression of superoxide dismutase 3 (SOD3); scale bars: 20 μm.

(**F**) FPH2 increased ATP production without significantly enhancing reactive oxygen species (ROS) production.

Murine chondrocytes were treated by 1 μM FPH2 for 48 hours and the control group was treated by 0.002% DMSO prior to the examinations.

All data are the mean ± SEM. **p* <0.05, ***p* < 0.01, ****p* <0.001.

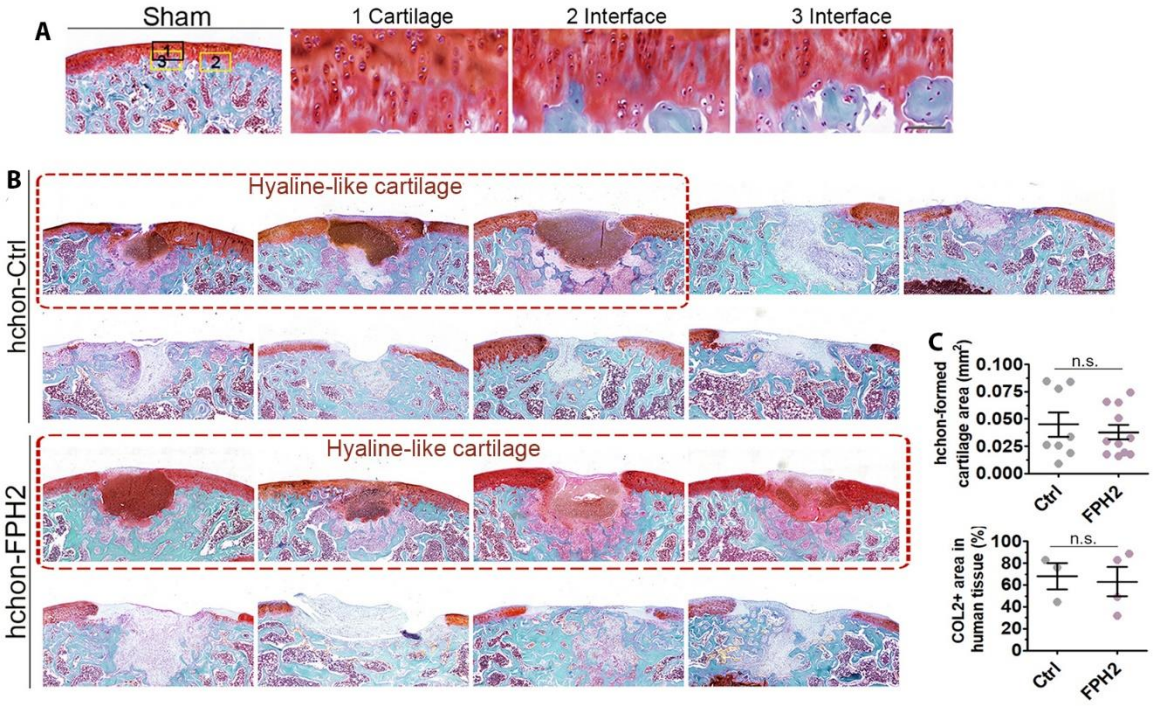

Fig. S9. FPH2 treatment promoted the formation of hyaline-like cartilage in vivo.

(**A**) Safranin O-fast green staining images of normal articular surfaces and cartilage-bone interfaces in rats, acting as the positive control; scale bar: 500 μm.

(**B**) Safranin O-fast green staining images of all joint samples implanted with human adult chondrocytes showing that FPH2-treated cells were more likely to form hyaline-like cartilage (4/8 *vs* 3/9); hchon-FPH2 and hchon-Ctrl group were implanted with human adult chondrocytes cultured with and without FPH2 respectively; scale bar: 500 μm.

(**C**) Quantitative comparison of the area of regenerative tissues formed by implanted cells (labeled by human Lamin A/C), and the comparison of the area positively marked with collagen type II (COL2) in the samples repaired with hyaline-like cartilage tissues (red boxes in Fig. S9B).

All data are the mean ± SEM. **p* <0.05, ***p* < 0.01, ****p* <0.001.

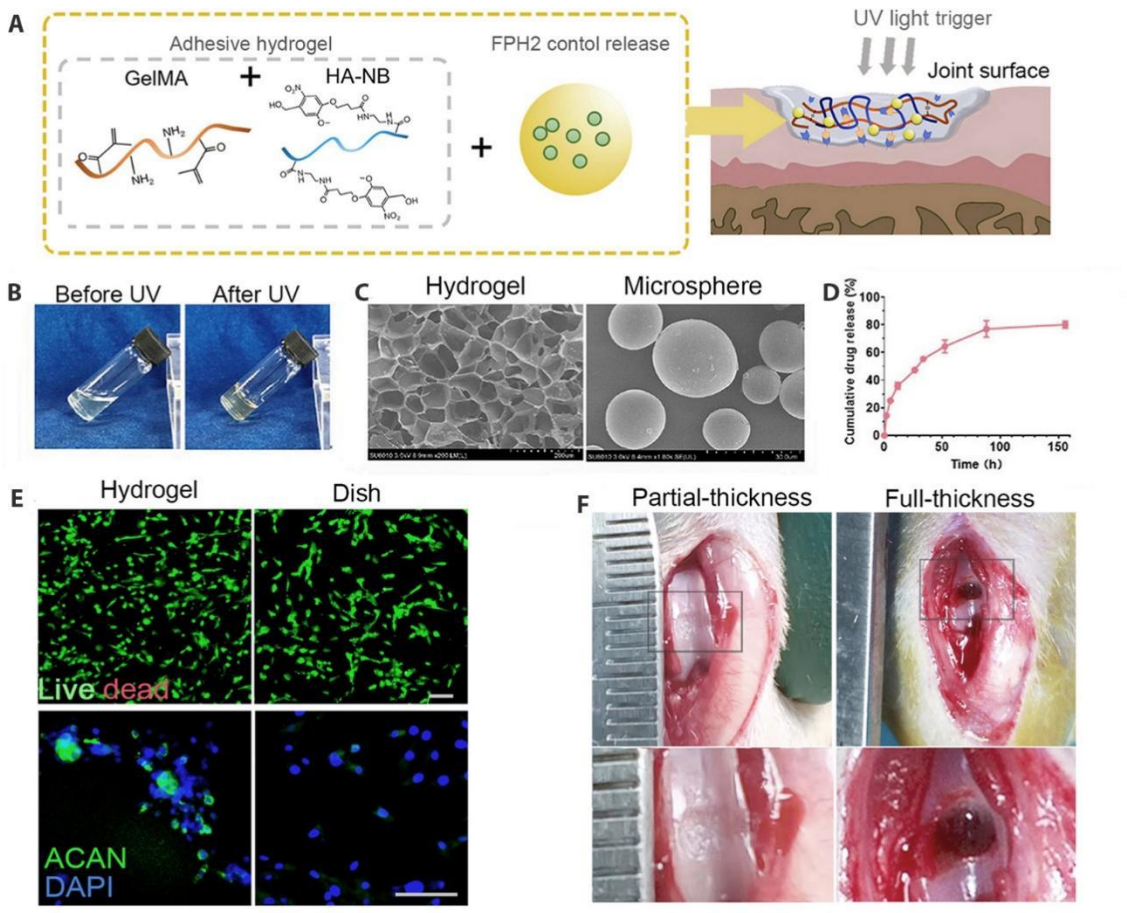

Fig. S10. FPH2-loaded hydrogel was applied to a partial-thickness cartilage injury.

(**A**) A schematic diagram illustrates the constitution of pharmaceutical hydrogel for the treatment of partial-thickness cartilage defects. Gelatin microspheres containing FPH2 were incorporated with light-triggered bio-adhesive hydrogel composed of gelatin methacrylate (GelMA) and hyaluronic acid linked with N-(2-aminoethyl)−4-(4-(hydroxymethyl)−2-methoxy-5-nitrosophenoxy) butanamide (HA-NB).

(**B**) Gross view of GelMA/HA-NB hydrogel before and after ultraviolet (UV)-triggered crosslinking.

(**C**) Representative scanning electronic microscopy (SEM) images of GelMA/HA-NB hydrogel and gelatin microspheres.

(**D**) The control release curve of FPH2 in gelatin microspheres.

(**E**) Representative images of live/dead and functional phenotype marker ACAN staining demonstrating that chondrocytes seeded on the hydrogel obtained a better functional phenotype than those on petri-dishes.

(**F**) Gross view comparison of partial- and full-thickness cartilage defects in rats' femurs.

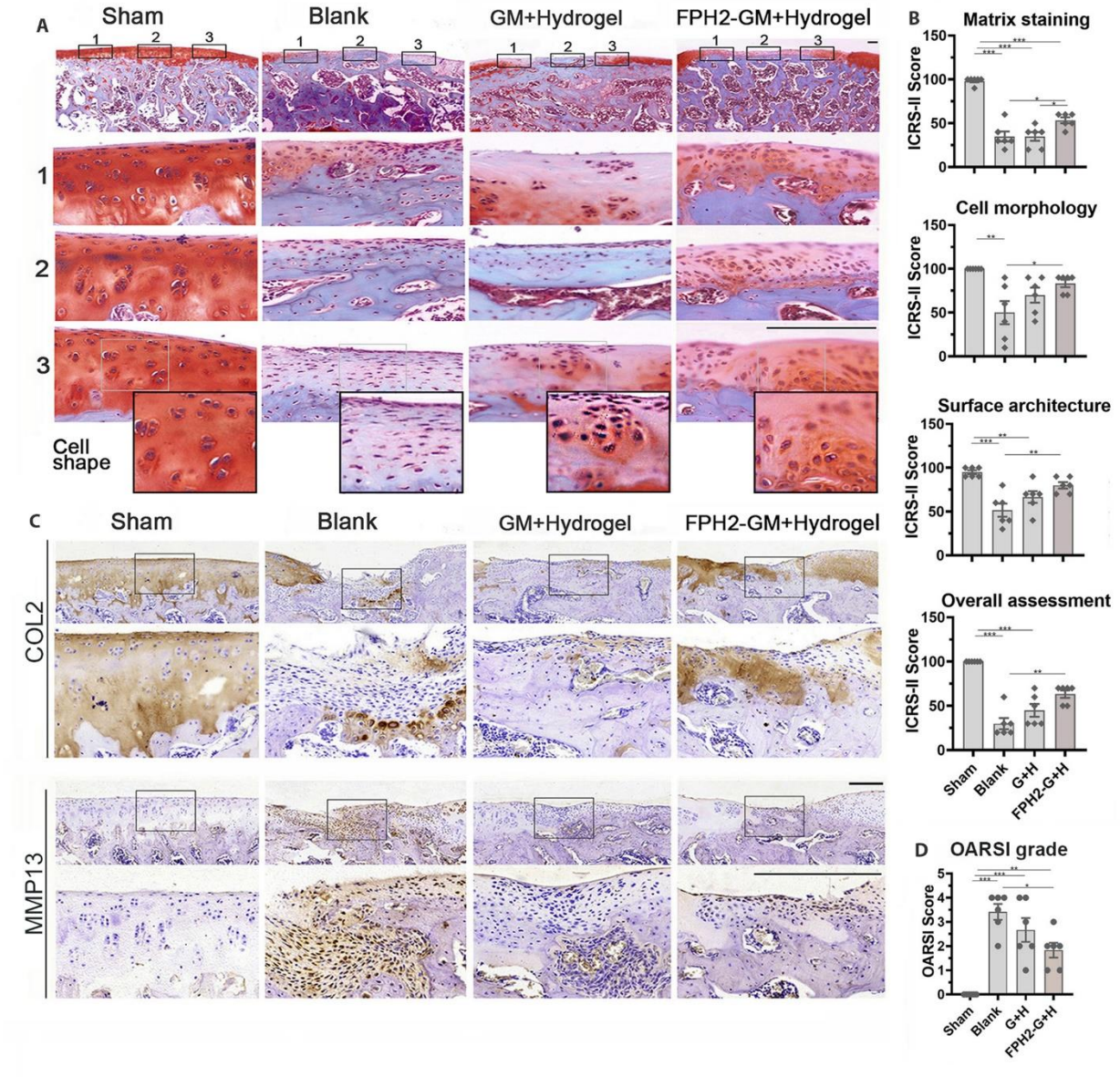

Fig. S11. FPH2-hydrogel ameliorated cartilage phenotype loss and prevented osteoarthritis.

(**A**)~(**B**) Representative safranin O-fast green staining images and ICRS-II scoring terms indicate an improved repair and an ameliorated cartilage phenotype loss at joint surfaces in FPH2-hydrogel group (n = 6 for each group). Blank group: defects without treatment; GM+Hydrogel group: blank gelatin microspheres with GelMA/HA-NB hydrogel; FPH2-GM+Hydrogel group: FPH2-loaded microspheres with GelMA/HA-NB hydrogel. Scale bars: 200μm

(**C**) Representative immunochemistry images of COL2 and matrix metalloproteinase 13 (MMP13) in repaired joints; scale bars: 200μm.

(**D**) OARSI grade scoring of repaired joints suggests that FPH2 delayed the development of early osteoarthritis.

All data are the mean ± SEM. **p* <0.05, ***p* < 0.01, ****p* <0.001.

Table S1. Donor information of human chondrocytes.

Sample	Donor age	Donor sex	Condition	Figures
Human young chondrocytes	17w	F	Embryonic cartilage	Fig. 2A and 2B
	4m	M	Polydactyly cartilage	Fig. 2E, 2F, 2G, S1A~S1C and S8
	11m	F	Polydactyly cartilage	
	11m	F	Polydactyly cartilage	
	1y1m	F	Polydactyly cartilage	
	8m	F	Polydactyly cartilage	Fig. 3, S2 and S3
	8m	F	Polydactyly cartilage	
	1y7m	F	Polydactyly cartilage	
	1y10m	M	Polydactyly cartilage	
Human adult chondrocytes and cartilage tissues	55y	F	Macroscopically normal tissue of osteoarthritis (OA) cartilage	Fig. S1A and S1B
	71y	F	Macroscopically normal tissue of OA cartilage	Fig. 2C (#1), 2D, 6 and S9
	74y	M	Macroscopically normal tissue of OA cartilage	Fig. 2C (#2), 2D, 6 and S9
	54y	M	Macroscopically normal tissue of OA cartilage	Fig. 2C (#3) and 2D
	65y	M	Macroscopically normal tissue of OA cartilage	Fig. S1D (#4), 2D, 6 and S9
	69y	F	Macroscopically normal tissue of OA cartilage	Fig. S1D (#5), 2D, 6 and S9
	75y	F	Macroscopically normal tissue of OA cartilage	Fig. S1D (#6), 2D, 6 and S9
	70y	M	Macroscopically normal tissue of OA cartilage	Fig. S1D (#7), 2D, 6 and S9
	76y	F	OA cartilage	Fig. 2H and 2I
	71y	M	OA cartilage	Fig. 3, S2 and S3
	67y	M	OA cartilage	
	70y	M	OA cartilage	
	74y	M	OA cartilage	
	60y	F	Macroscopically normal tissue of OA cartilage	Fig.4E, 4F and 5G~5I
	23y	M	Cartilage injury	

Table S2. Candidate FPH2 targets, predicted by Similarity Ensemble Approach.

Rank	Target	Species	P-Value	Z-score
1	CPT1B	Human	8.0×10^{-53}	93.0806
2	CPT1A	Human	6.3×10^{-50}	87.8801
3	Cpt1a	Rat	9.9×10^{-49}	85.7292
4	Nlrp3	Mouse	3.0×10^{-39}	68.7108
5	DUS2	Human	2.3×10^{-36}	63.5209
6	Cpt2	Rat	4.1×10^{-33}	57.6797
7	CPT2	Human	1.2×10^{-31}	55.0573
8	PDE4A	Pig	1.9×10^{-26}	45.7239
9	Qpct	Mouse	7.9×10^{-25}	42.8201
10	CFTR	Human	2.4×10^{-23}	40.1565

Data S1. The list of 2178 candidate drugs in the primary screen.

Data S2. Top 300 marker genes of the 8 clusters in single-cell transcriptomics.

Data S3. Differentially regulated metabolites in FPH2 group relative to the control.